

Shishkin mesh simulation: A new stabilization technique for convection-diffusion problems and complementary experiments

Bosco García-Archilla*

June 7, 2021

Abstract

We present together in this document the paper B. García-Archilla, Shishkin mesh simulation: A new stabilization technique for convection-diffusion problems, *Comput. Methods Appl. Mech. Engrg.*, 256 (2013), 1–16, and the manuscript B. García-Archilla, Shishkin mesh simulation: Complementary experiments, which contains some of the experiments that, for the sake of brevity were not included in the first one. *This second paper with complementary experiments is neither self-contained nor intended to be published in any major journal*, but is intended to be accessible to anyone wishing to learn more on the performance of the SMS method. Following a principle of reproducible computational research, the source codes of the experiments in the present papers are available from the author on request or on "http://personal.us.es/bga/bga_files/software_bga.html". Excluded are the codes corresponding to Example 7 which is subject of current research

*Departamento de Matemática Aplicada II, Universidad de Sevilla, Sevilla, Spain. Research supported by Spanish MEC under grant MTM2009-07849 (bosco@esi.us.es)

Shishkin mesh simulation: A new stabilization technique for convection-diffusion problems

Bosco García-Archilla¹

Abstract

A new stabilization procedure is presented. It is based on a simulation of the interaction between the coarse and fine parts of a Shishkin mesh, but can be applied on coarse and irregular meshes and on domains with nontrivial geometries. The technique, which does not require adjusting any parameter, can be applied to different stabilized and non stabilized methods. Numerical experiments show it to obtain oscillation-free approximations on problems with boundary and internal layers, on uniform and nonuniform meshes and on domains with curved boundaries.

Key words. Convection-dominated problems. Stabilized methods. Finite-element methods. Galerkin method. SUPG method.

1 Introduction

The numerical solution of convection-diffusion problems when convection dominates is, despite more than 30 years of research, a challenging problem nowadays. Standard finite-element or finite-difference methods typically suffer from unphysical or spurious oscillations unless meshes are taken so fine that are useless for all practical purposes. The reason is the presence of layers or thin regions where solutions change fast. Modification of standard methods, known as stabilized methods have been proposed in the literature, from upwind methods 35 years ago [45], to strongly-consistent stabilized methods like the streamline upwind/Petrov-Galerkin (SUPG) method [7], also known as the streamline diffusion finite element method (SDFEM), or the Galerkin least-squares (GALS) method [24]. More recently, local projection stabilization (LPS) methods, [4], [6], [18], continuous interior penalty (CIP) methods [8], or discontinuous Galerkin (DG) methods [23], [35] have been introduced, to cite a few of the many techniques proposed (see [36], [38] for a survey of methods). It must be noticed, however, that computational studies (see e.g., [2], [26]) find it hard to put a particular method above the others. It must be also mentioned that most of these methods depend on at least one parameter about which there is no unanimous agreement on its optimal choice in practical problems [27].

¹Departamento de Matemática Aplicada II, Universidad de Sevilla, 41092 Sevilla, Spain. Research supported by Spanish MEC under grant MTM2009-07849 (bosco@etsi.us.es)

A different approach is to use layer-adapted meshes. Among these we cite Shishkin meshes (described below) [31], [37], which have received considerable attention in recent years [14], [15], [16], [28], [32], [33] [39], [43] and [47]. However, it is generally acknowledged that the main drawback of Shishkin meshes is the difficulty to design them on domains with nontrivial geometries, although some works overcoming this difficulty can be found in the literature [46], [28].

The method we propose, however, does not suffer from the above indicated drawbacks: It does not depend on parameters and, although it is based on the idea of simulating a Shishkin mesh, the experiments we present show it produces excellent results on domains with nontrivial geometries.

We consider the problem

$$-\varepsilon \Delta u + b \cdot \nabla u + cu = f, \quad \text{in } \Omega, \quad (1)$$

$$u = g_1, \quad \text{in } \partial\Omega_D, \quad \frac{\partial u}{\partial n} = g_2, \quad \text{in } \partial\Omega_N. \quad (2)$$

Here, Ω is a bounded domain in \mathbb{R}^d , $d = 1, 2, 3$, its boundary $\partial\Omega$ being the disjoint union of Γ_D and Γ_N , b and c are given functions and $\varepsilon > 0$ is a constant diffusion coefficient. We assume that $\Gamma^- \subset \partial\Omega_D$, Γ^- being the inflow boundary of $\Omega \subset \mathbb{R}^d$, i.e., the set of points $x \in \partial\Omega$ such that $b(x) \cdot n(x) < 0$.

It is well-known if $\varepsilon \ll \sup\{|b(x)| \mid x \in \Omega\}$ ($|\cdot|$ being the euclidean norm) boundary layers are likely to develop along $\partial\Omega \setminus \Gamma^-$, although they have different structure on $\Gamma^0 = \{x \in \partial\Omega \mid b(x) \cdot n(x) = 0\}$ and $\Gamma^+ = \{x \in \partial\Omega \mid b(x) \cdot n(x) > 0\}$. As already mentioned, these boundary layers, when present, are responsible of the spurious oscillations that pollute the numerical approximations obtained with standard methods unless extremely fine meshes are used. For uniform meshes, oscillations typically disappear when the *mesh Péclet number*

$$\text{Pe} = \frac{\|b\|_{L^\infty(\Omega)^2} h}{2\varepsilon}$$

(h being the mesh size) is of the order of 1.

Let us briefly describe now the idea of the method we propose in the following simple problem:

$$L(u) \equiv -\varepsilon u''(x) + b(x)u'(x) + c(x) = f(x), \quad 0 < x < 1, \quad (3)$$

$$u(0) = u(1) = 0. \quad (4)$$

In (3) we assume that b , c and f are sufficiently smooth functions, and that

$$0 < \beta < \min_{x \in [0,1]} b(x), \quad 0 \leq \min_{x \in [0,1]} c(x). \quad (5)$$

The standard Galerkin linear finite-element method for (3-4) on a partition or mesh $0 = x_0 < x_1 < \dots < x_J = 1$ of $[0, 1]$ obtains a continuous piecewise linear approximation $u_h(x)$ to u . As it is customary, h denotes the mesh diameter, $h = \max_{1 \leq j \leq J} h_j$, where $h_j = x_j - x_{j-1}$, for $j = 1, \dots, J$. The approximation can be expressed as $U(x) = u_1 \varphi_1(x) + \dots + u_{J-1} \varphi_{J-1}(x)$, where the $\varphi_j(x)$ are

the basis or hat (piecewise linear) functions taking value 1 at the node x_j and 0 in the rest of the nodes of the partition (thus, $U(x_j) = u_j$). The values u_j , $j = 1, \dots, J-1$, are obtained by solving the linear system of equations

$$a(u_h, \varphi_i) = (f, \varphi_i), \quad i = 1, \dots, J-1, \quad (6)$$

where, a is the bilinear form associated with (3), which is given by

$$a(v, w) = \varepsilon(v', w') + (bv' + c, w),$$

(\cdot, \cdot) being the standard inner product in $L^2(0, 1)$,

$$(f, g) = \int_0^1 f(x)g(x) dx.$$

The Shishkin mesh with $J = 2N$ nodes is composed of two uniform meshes with N subintervals on each side of the transition point $x_N = 1 - \sigma$, where

$$\sigma = \min\left(\frac{1}{2}, \frac{2}{\beta}\varepsilon \log N\right),$$

for an adequate constant β , that is, $x_j = j(1 - \sigma)/N$, for $j = 0, \dots, N$, and $x_{N+j} = x_N + j\sigma/N$, for $j = 1, \dots, N$. Let us consider the coarse and fine grid parts of the Galerkin approximation given by

$$\begin{aligned} U_c(x) &= u_1\varphi_1(x) + \dots + u_{N-1}\varphi_{N-1}(x), \\ U_f(x) &= u_{N+1}\varphi_{N+1}(x) + \dots + u_{2N-1}\varphi_{2N-1}(x), \end{aligned}$$

so that $U_c + u_N\varphi_N + U_f$ is the Galerkin approximation on the Shishkin mesh. Since for $i = 1, \dots, J-1$, the support of the basis function φ_i is $[x_{i-1}, x_{i+1}]$, we have $a(U_c, \varphi_{N+j}) = 0$ and $a(U_f, \varphi_j) = 0$, for $j = 1, \dots, N-1$. Consequently the system (6) on the Shishkin mesh can be rewritten as

$$a(U_c, \varphi_i) = (f, \varphi_i), \quad i = 1, \dots, N-2, \quad (7)$$

$$a(U_c, \varphi_i) + u_N a(\varphi_N, \varphi_i) = (f, \varphi_i), \quad i = N-1, \quad (8)$$

$$a(U_c, \varphi_N) + u_N a(\varphi_N, \varphi_N) + a(U_f, \varphi_N) = (f, \varphi_N), \quad (9)$$

$$u_N a(\varphi_N, \varphi_i) + a(U_f, \varphi_i) = (f, \varphi_i), \quad i = N+1, \dots, 2N-1. \quad (10)$$

We notice that were it not for the presence of the $u_N a(\varphi_N, \varphi_i)$ in (8), the system (7–8) would be the equations

$$a(U, \varphi_i) = (f, \varphi_i), \quad i = 1, \dots, N-1, \quad (11)$$

of the Galerkin approximation $U = U_1\varphi_1 + \dots + U_{N-1}\varphi_{N-1}$ for the problem

$$-\varepsilon u''(x) + b(x)u'(x) + c(x) = f(x), \quad 0 < x < 1 - \sigma, \quad (12)$$

$$u(0) = u(1 - \sigma) = 0. \quad (13)$$

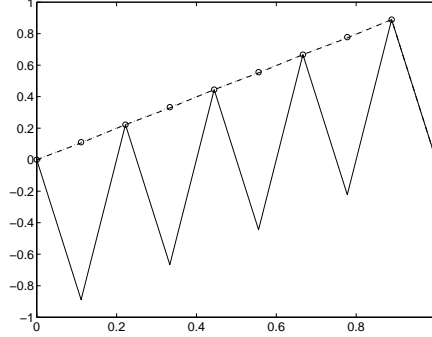


Figure 1: Galerkin approximation on a uniform mesh with $N = 9$ (continuous line) to the solution of (12–13) with $\varepsilon = 10^{-8}$, $\sigma = 4\varepsilon \log(2 * N)$, $b = f = 1$, and $c = 0$. The U_c part of the Galerkin approximation on a Shishkin mesh with $J = 18$ (broken line) for same ε and f . Circles are the values of the true solution on the nodes.

The Galerkin approximation U for this problem, unless $\varepsilon N > 1/2$, is likely to have spurious oscillations of large amplitude as we show in Fig. 1 for $\varepsilon = 10^{-8}$, $\sigma = 4\varepsilon \log(J)$, $b(x) = f(x) = 1$, $c = 0$ and $N = 9$. It is however the presence of $u_N a(\varphi_N, \varphi_i)$ in equation (8) that suppresses the oscillations, as we can see in Fig. 1, where the component U_c of the Galerkin approximation on a Shishkin grid with $J = 2N = 18$ is also shown (discontinuous line) together with the true solution at the nodes of the coarse part of the mesh.

It is remarkable that just by adding the value

$$\alpha^* = u_N a(\varphi_{N-1}, \varphi_N) \quad (14)$$

to the last equation of the Galerkin method for (12–13) we get the oscillation-free approximation U_c . Obviously, in order to have the value of α^* we have to solve the whole system (7–10). In the present paper, we introduce a technique to approximate α^* without the need to compute the whole approximation on the Shishkin grid. In Fig. 1, the approximation computed with the estimated α^* is indistinguishable from U_c . Numerical experiments in the present paper show that, in two-dimensional problems, the oscillation-free approximation on a coarse mesh can be obtained by this technique at half the computational cost of a Shishkin grid, and a more substantial gain can be expected in three-dimensional problems.

Furthermore, this technique can be extended when the grid is no part of any Shishkin grid, while, at the same time, managing to get rid of the spurious oscillations. This allows to obtain accurate approximations on domains with non trivial boundaries, where Shishkin meshes may be difficult to construct. In spite of this, we call the new technique *Shishkin mesh simulation* (SMS), since it was derived, as described above, in an attempt to simulate Shishkin grids.

We must mention, however, that in the present paper we only consider the case of dominant convection, both in the analysis and in the numerical experi-

ments. The question of how to modify the method (if necessary) when the mesh Péclet number Pe tends to one will be addressed elsewhere.

It is well-known that the Galerkin method is a far from ideal method in convection-diffusion problems. Let us also notice that despite the good properties of stabilized methods developed in recent years, the SUPG method is still considered the standard approach [27]. For this reason, in the numerical experiments presented below, we compare the new method with the SUPG method.

The rest of the paper is as follows. In Section 2 we describe the SMS method in detail. In Section 3 we present a limited analysis of the new technique. Section 4 contains the numerical experiments and Section 5 the conclusions.

2 The new technique: Shishkin mesh simulation

2.1 The one-dimensional case

We consider (3–4) satisfying (5). Given a partition $0 = x_0 < x_1 < \dots < x_J = 1$, of $[0, 1]$, we denote by X_h the space of continuous piecewise linear functions, and by V_h the subspace of X_h of functions taking zero values at $x = 0$ and $x = 1$, so that we can express

$$X_h = \text{span}\{\varphi_0\} \oplus V_h \oplus \text{span}\{\varphi_J\}.$$

We consider the operator L_h given by

$$L_h(v_h) = bv'_h + cv_h, \quad v_h \in V_h.$$

(See also Remark 1 below). We denote by $u_h \in V_h$ the standard Galerkin linear finite-element approximation, and by \tilde{u}_h the SMS approximation. This is found as the solution of the least-squares problem

$$\min_{\tilde{u}_h \in V_h, \alpha \in \mathbb{R}} \|L_h(\tilde{u}_h) - f\|_{L^2(0, x_{J-1})}, \quad (15)$$

subject to the restriction

$$a(\tilde{u}_h, \varphi_h) + \alpha \varphi_h(x_{J-1}) = (f, \varphi), \quad \varphi_h \in V_h. \quad (16)$$

Observe that since $\varphi_h(x_{J-1}) = 0$ for φ_h not proportional to φ_{J-1} , and recalling how we defined α^* in (14), equation (16) is similar to (7–8), and then, the least-squares problem (15) is the way of finding the value α hopefully close to α^* .

Notice also that the restriction (16) is, in fact, a set of as many independent restrictions as interior nodes or nodal basis functions in V_h . Consequently, in the optimality conditions, there must be a Lagrange multiplier for every interior node. We gather all this multipliers in a function $z_h \in V_h$ whose value at every node is that of the corresponding Lagrange multiplier. Thus, the optimality conditions of the SMS approximation can be written as the following linear

problem: find $\tilde{u}_h, z_h \in V_h$ and $\alpha \in \mathbb{R}$ such that

$$(L_h(\tilde{u}_h), L_h(\varphi_h))_{L^2(0, x_{J-1})} - a_h(\varphi_h, z_h) = (f, L_h(\varphi_h))_{L^2(0, x_{J-1})}, \quad \varphi_h \in V_h, \quad (17)$$

$$z_h(x_{J-1}) = 0, \quad (18)$$

$$a(\tilde{u}_h, \varphi_h) + \alpha \varphi_h(x_{J-1}) = (f, \varphi_h), \quad \varphi_h \in V_h, \quad (19)$$

where here and in the sequel $(\cdot, \cdot)_{L^2(I)}$ denotes the standard inner product in $L^2(I)$.

Remark 1 Observe that for linear elements the operator L_h coincides with

$$L_h(v_h) = \sum_{j=1}^J (-\varepsilon v_h'' + b v_h' + c v_h)|_{(x_{j-1}, x_j)}, \quad (20)$$

that is, L applied element by element. This expression of L_h is better suited to the SMS method for higher-order elements, a topic that will be studied elsewhere.

Remark 2 The fact that the approximation \tilde{u}_h is found by solving the least-squares problem (15) may suggest a possible relation with the GALS method (compare for example least-squares problem (15) with that in [36, p. 327]). However, they are very different methods, since for the examples in Section 4 in the present paper, SUPG and GALS methods are identical (see e.g. [24]), and, as shown in Section 4, the SMS method and the SUPG method produce markedly different results.

2.2 The multidimensional case

We will assume that $b(x) \neq 0$ for $x \in \Omega$, and that every characteristic (i.e., solution of $dx/dt = b(x)$) in Ω enters and leaves Ω in finite time. Also for simplicity, we will assume that the domain Ω in (1-2) has a polygonal or polyhedral boundary.

Let \mathcal{T}_h a triangulation of it, that is, a partition of the closure $\overline{\Omega}$ of Ω in n -simplices with only faces and vertices in common. For every $\tau \in \mathcal{T}_h$, let $\mathcal{N}(\tau)$ be the set of its vertices, and let $\mathcal{N}_h = \cup_{\tau \in \mathcal{T}_h} \mathcal{N}(\tau)$ be the set of vertices of \mathcal{T}_h .

Similarly to the one-dimensional case, let X_h the space of continuous piecewise linear polynomials. We express

$$X_h = X_h^- \oplus V_h \oplus X_h^+,$$

where $\varphi_h = 0$ on Γ_D if $\varphi_h \in V_h$, and for φ_h in X_h^- (resp. X_h^+), if $\varphi_h(x) \neq 0$ for $x \in \mathcal{N}_h$, then $x \in \Gamma^-$ (resp. $\Gamma_D \setminus \Gamma^-$). In the standard Galerkin method, first an element $u_h^D \in X_h^- \oplus X_h^+$ is selected such that the restriction $u_h^D|_{\Gamma_D}$ to Γ_D is a good approximation to the Dirichlet data g_1 in (2). This restriction is typically the interpolant or the $L^2(\Gamma_D)$ -projection onto the restrictions to Γ_D of functions in X_h . Then, the Galerkin approximation $u_h \in u_h^D + V_h$ satisfies

$$a(u_h, \varphi_h) = (f, \varphi_h) + \varepsilon \langle g_2, \varphi_h \rangle_{\Gamma_N}, \quad \forall \varphi_h \in V_h, \quad (21)$$

where here and in the sequel, $\langle \cdot, \cdot \rangle_\Gamma$ denotes the L^2 inner product on $\Gamma \subseteq \partial\Omega$, and

$$a(v, w) = \varepsilon(\nabla v, \nabla w) + (b \cdot \nabla v + cv, w), \quad v, w \in H^1(\Omega).$$

For the new method, similarly to the one-dimensional case, we consider

$$L_h(v_h) = b \cdot \nabla v_h + cv_h.$$

In order to describe the new approximation, we must set up the multidimensional version of the last interval (x_{J-1}, x_J) in the one-dimensional case. For this purpose we denote

$$\Gamma_D^{0+} = (\Gamma^+ \cup \Gamma^0) \cap \Gamma_D.$$

We consider a suitable Ω_h^+ with $\Gamma_D^{0+} \subset \partial\Omega_h^+$ (to be specified below) and let us denote by \mathcal{N}_δ and \mathbb{N}_δ the set of vertices in $\partial\Omega_h^+ \setminus \Gamma_D$ and their indices, respectively, that is

$$\mathcal{N}_\delta = \mathcal{N}(\partial\Omega_h^+ \setminus \Gamma_D), \quad \mathbb{N}_\delta = \{j \in \mathbb{N} \mid x_j \in \mathcal{N}_\delta\},$$

and by $\mathbb{R}^{\mathbb{N}_\delta}$ we will refer to the set of real vectors of the form $(t_j)_{j \in \mathbb{N}_\delta}$. The points in \mathcal{N}_δ and the set Ω_h^+ will play a role similar to that of x_{J-1} and (x_{J-1}, x_J) in the one-dimensional case. This can be seen in Fig. 2, where, shadowed in grey, we show the set Ω_h^+ for a triangulation of the unit square for $b = [1, 1]^T$, with $\Gamma_D = \partial\Omega$, so that $\Gamma^0 \cup \Gamma^+$ consists of the sides $y = 1$ and $x = 1$. We show the points in \mathcal{N}_δ marked with circles.

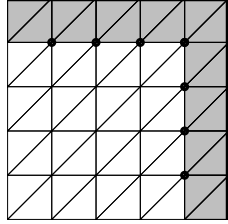


Figure 2: A triangulation of the unit square with $\Gamma^0 \cup \Gamma^+$ marked with a thicker line, the set Ω_h^+ in grey and the the points of \mathcal{N}_δ with circles.

The approximation $\tilde{u}_h \in u_h^D + V_h$, is then found by solving the least-squares problem

$$\min_{\tilde{u}_h \in u_h^D + V_h, t \in \mathbb{R}^{\mathbb{N}_\delta}} \|L_h(\tilde{u}_h) - f\|_{L^2(\Omega \setminus \Omega_h^+)}, \quad (22)$$

subject to the restriction

$$a(\tilde{u}_h, \varphi_h) + \sum_{j \in \mathbb{N}_\delta} t_j \varphi_h(x_j) = (f, \varphi_h) + \varepsilon \langle g_2, \varphi_h \rangle_{\Gamma_N}, \quad \varphi_h \in V_h. \quad (23)$$

The optimality conditions of this problem can be written as the following linear problem: find $\tilde{u}_h \in u_h^D + V_h$, $z_h \in V_h$ and $t \in \mathbb{R}^{\mathbb{N}_\delta}$ such that

$$(L_h(\tilde{u}_h), L_h(\varphi_h))_{L^2(\Omega \setminus \Omega_h^+)} - a_h(\varphi_h, z_h) = (L_h(\varphi_h), f)_{L^2(\Omega \setminus \Omega_h^+)}, \quad \varphi_h \in V_h, \quad (24)$$

$$z_h(x_j) = 0, \quad j \in \mathbb{N}_\delta, \quad (25)$$

$$a(\tilde{u}_h, \varphi_h) + \sum_{j \in \mathbb{N}_\delta} t_j \varphi_h(x_j) = (f, \varphi_h) + \varepsilon \langle g_2, \varphi_h \rangle_{\Gamma_N}, \quad \varphi_h \in V_h, \quad (26)$$

where, as in the one-dimensional case, z_h is the Lagrange multiplier of restriction (23).

Let us specify now the set Ω_h^+ . The obvious choice of setting $\Omega_h^+ = B_h$ where

$$B_h = \bigcup_{\tau \cap (\Gamma_D^{0+}) \neq \emptyset} \tau,$$

as in Fig. 2, may lead to an unstable method if there are nodes $x \in \mathcal{N}_h$ interior to B_h , as it can be easily checked in a numerical experiment. To understand why

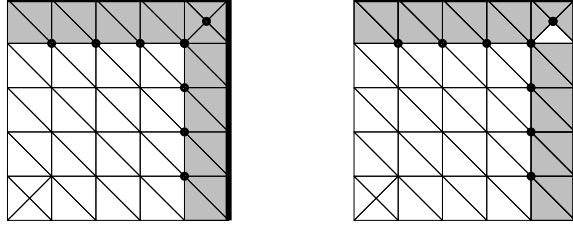


Figure 3: A triangulation of the unit square with $\Gamma^0 \cup \Gamma^+$ marked with a thicker line and the points of \mathcal{N}_δ with circles. In grey, the sets B_h (left plot) and Ω_h^+ (right plot) for $b = [1, 1]^T$.

in such a case the SMS method may be unstable, consider the limit case $\varepsilon = 0$, b constant and $c = 0$ (so that the bilinear form a is skew-symmetric) and consider a mesh as that depicted in Fig. 3, where there is one node x_i interior to B_h who has only one neighbour node $x_k \in \mathcal{N}_\delta$. Then, on the one hand, the basis function φ_i of the node x_i satisfies that $a_h(\varphi_i, \varphi_h) = 0$ for all $\varphi_h \in V_h$, except when φ_h is a multiple of the basis function φ_k of the node x_k . Furthermore, since the support of φ_i is contained in B_h , we have that $\|L_h(\varphi_i)\|_{L^2(\Omega \setminus B_h)} = 0$. Consequently, taking $\tilde{v}_h = \varphi_i$, $z_h = 0$, $t_l = 0$ for $l \neq k$ and $t_k = -a(\varphi_i, \varphi_k)$ we have a nontrivial solution of

$$(L_h(\tilde{v}_h), L_h(\varphi_h))_{L^2(\Omega \setminus \Omega_h^+)} - a_h(\varphi_h, z_h) = 0, \quad \varphi_h \in V_h, \quad (27)$$

$$z_h(x_j) = 0, \quad j \in \mathbb{N}_\delta, \quad (28)$$

$$a(\tilde{v}_h, \varphi_h) + \sum_{j \in \mathbb{N}_\delta} t_j \varphi_h(x_j) = 0, \quad \varphi_h \in V_h, \quad (29)$$

if we set $\Omega_h^+ = B_h$. It can be easily checked that this is also the case if the node x_i interior to B_h is connected to more than one node in \mathcal{N}_δ . For $\varepsilon > 0$, one can expect a unique solution but, as we have checked in practice, it is a solution where $\tilde{u}(x_i) = O(1/\varepsilon)$.

To avoid this situation we remove from B_h the upwind triangle of any interior point. More precisely, for every node $x_i \in \mathcal{N}_h$, let us denote by $\tau_-(x_i)$ its upwind triangle, that is

$$\tau_-(x_i) = \{\tau \in \mathcal{T}_h \mid \{x_i - \lambda b\} \cap \tau \neq \emptyset, \quad \lambda \rightarrow 0\}.$$

Then we define

$$\Omega_h^+ = B_h \setminus \left(\bigcup_{x_i \in \mathcal{N}_h \cap \overset{\circ}{B}_h} \tau_-(x_i) \right).$$

If there are two upwind triangles because $x_j - \lambda b$ is and edge for λ smaller than some λ_0 , we may select the first one of them after ordering all the elements.

With this choice of Ω_h^+ , as we will show in Section 3.2.1, the few cases where there are nontrivial solutions of (27–29) have an easy fix from the computational point of view. We also note that a slightly different choice of Ω_h^+ is taken in Example 7 in Section 4, where the vector field b has closed integral curves.

2.3 Further Extensions

In the same way that the Shishkin meshes are not restricted to the standard Galerkin method, the new technique, originally motivated by Shishkin meshes, is not restricted to the Galerkin method either. In this section we comment on how to use it with some other methods of widespread use, such as the SUPG, GALS, LPS and CIP methods.

In these methods the approximation $u_h \in u_h^D + V_h$, instead of satisfying (21), satisfies

$$a_h(u_h, \varphi_h) = (f, \varphi_h)_h + \varepsilon \langle g_2, \varphi_h \rangle_{\Gamma_N}, \quad \forall \varphi_h \in V_h, \quad (30)$$

where a_h and $(\cdot, \cdot)_h$ are mesh-dependent bilinear forms. For the SUPG method they are given by

$$a_h(v_h, \varphi_h) = a(v_h, \varphi_h) + \sum_{\tau \in \mathcal{T}_h} \delta_\tau (L|_\tau(v_h), b \cdot \varphi_h)_\tau, \quad (31)$$

$$(f, \varphi_h)_h = (f, \varphi_h) + \sum_{\tau \in \mathcal{T}_h} \delta_\tau (f, b \cdot \varphi_h)_\tau, \quad (32)$$

where δ_τ is an adequately chosen parameter and $L|_\tau$ denotes L restricted to τ . In the GALS method the term $b \cdot \nabla \varphi_h$ is replaced by $L|_\tau(\varphi_h)$ (see e. g., [36] for a full description of these methods). The extension of the SMS technique to these methods is as follows: we solve the least-squares problem (22) but we replace the restriction (23) by

$$a_h(\tilde{u}_h, \varphi_h) + \sum_{j \in \mathbb{N}_\delta} t_j \varphi_h(x_j) = (f, \varphi_h)_h + \varepsilon \langle g_2, \varphi_h \rangle_{\Gamma_N}, \quad \varphi_h \in V_h. \quad (33)$$

In the numerical experiments in the present paper, we only consider the SMS for the SUPG method. To distinguish it from the SMS method in the previous section, we will refer to them as *Galerkin-based* and *SUPG-based* SMS methods.

We could also consider the extension to higher-order finite-element methods. The extension seems straightforward since it consists in replacing the approximation space V_h by piecewise quadratics or piecewise cubics (together with L_h in (20)). Numerical experiments (not reported here) indicate that this straightforward extension does not give as good results as the piecewise linear elements, at least for one-dimensional problems. The reason seems to be the need to redefine the set Ω_h^+ for higher-order elements. This will be subject of future studies.

3 Analysis of the SMS method

3.1 The one-dimensional case

Some understanding of why the new method is able to suppress or, at least, dramatically reduce the spurious oscillations of standard approximations can be gained by analyzing the problem (3–4) when b is a positive constant and $c = 0$. We do this first for the Galerkin method.

The Galerkin method.

We first consider the limit case $\varepsilon = 0$. In this case, it is easy to check that the Galerkin approximation satisfies the equations

$$\frac{b}{2}(u_{j+1} - u_{j-1}) = f_j \equiv \int_{x_{j-1}}^{x_{j+1}} f(x)\varphi_j(x) dx, \quad j = 1, \dots, J-1. \quad (34)$$

Thus, summing separately odd and even-numbered equations we obtain the following expressions,

$$u_{2j} = u_0 + \frac{2}{b} \sum_{i=1}^j f_{2i-1}, \quad j = 1, \dots, (J' - 1)/2, \quad (35)$$

$$u_{2j-1} = u_{J'} - \frac{2}{b} \sum_{i=j}^{(J'-1)/2} f_{2i}, \quad j = 1, \dots, (J' - 1)/2, \quad (36)$$

where, here and in the rest of this section

$$J' = \begin{cases} J, & \text{if } J \text{ is odd,} \\ J - 1, & \text{if } J \text{ is even.} \end{cases}$$

We notice that when J is odd, the expressions in (35–36) are the discrete counterparts of the problems

$$bu_x = f, \quad 0 < x < 1, \quad u(0) = 0, \quad (37)$$

$$bu_x = f, \quad 0 < x < 1, \quad u(1) = 0, \quad (38)$$

which, unless f has zero mean, have different solutions. Thus, since for sufficiently smooth f the expressions (35–36) are consistent with (37–38), oscillations in the numerical approximation are bound to occur whenever f is not of zero mean. For J even, it is easy to check that the Galerkin equations (34) have no solution unless $f_1 + f_3 + \dots + f_{J-1} = 0$, in which case the solution is not unique. Thus for J even the Galerkin method is not stable.

However, for J odd, the Galerkin method is stable in the following sense

$$\|u_h\|_\infty \leq \frac{2}{b} \|f\|_{-h}, \quad (39)$$

where

$$\|f\|_{-h} = \|S_h\|_\infty, \quad (40)$$

and

$$S_{2j} = \sum_{i=1}^j f_{2i-1}, \quad S_{2j-1} = \sum_{i=j}^{(J'-1)/2} f_{2i}, \quad j = 1, \dots, (J'-1)/2. \quad (41)$$

The SMS technique. Here the equations are

$$\frac{b}{2}(\tilde{u}_{j+1} - \tilde{u}_{j-1}) + \alpha \delta_{J-1}(j) = f_j \quad j = 1, \dots, J-1, \quad (42)$$

where δ_{J-1} denotes Dirac's delta function

$$\delta_{J-1}(j) = \begin{cases} 0, & \text{if } j \neq J-1, \\ 1, & \text{if } j = J-1. \end{cases}$$

As Proposition 1 below shows, the SMS method is stable independently of the parity of the grid. To prove stability we will consider the auxiliary function $q_h \in V_h$ whose nodal values are

$$q_j = -\frac{1 - (-1)^j}{b}, \quad j = 1, \dots, J-1. \quad (43)$$

It is easy to check that when J is odd q_h satisfies

$$a(q_h, \varphi_h) = \varphi_h(x_{J-1}), \quad \varphi_h \in V_h, \quad (44)$$

whereas when J is even it satisfies

$$a(q_h, \varphi_h) = 0, \quad \varphi_h \in V_h. \quad (45)$$

Proposition 1 *There exist a positive constant C such that for $\varepsilon = 0$ the SMS approximation \tilde{u}_h satisfies*

$$\|\tilde{u}_h\|_\infty \leq \frac{6}{b} \left(\|f\|_{-h} + \frac{h}{6J} |r| \right), \quad (46)$$

where $r = (f, L_h(q_h))_{L^2(0, x_{J-1})}$.

Proof. Recall that the SMS approximation \tilde{u}_h is part of the solution $(\tilde{u}_h, \alpha, z_h)$ of system (17–19). Due to (44), (45) and (18) we have that $a(q_h, z_h) = 0$, so that taking $\varphi_h = q_h$ in (17) we have

$$(L_h(\tilde{u}_h), L_h(q_h))_{L^2(0, x_{J-1})} = (f, L_h(q_h))_{L^2(0, x_{J-1})}. \quad (47)$$

On the other hand, we notice that $L(q_h) = 2(-1)^j/h_j$, for $x \in (x_{j-1}, x_j)$ and $j = 1, \dots, J-1$, so that equation (47) becomes

$$2 \sum_{j=1}^{J-1} (-1)^j b \frac{\tilde{u}_j - \tilde{u}_{j-1}}{h_j} = 2 \sum_{j=1}^{J-1} (-1)^j \frac{1}{h_j} \int_{x_{j-1}}^{x_j} f(x) dx. \quad (48)$$

To prove (46) we treat the cases J odd and J even separately. For J odd, we notice that since the equations in (42) are those of the Galerkin method except for the last one, applying the stability estimate (39) we have

$$\|\tilde{u}_h\|_\infty \leq \frac{2}{b} (\|f\|_{-h} + |\alpha|). \quad (49)$$

Also, since $\tilde{u}_h = u_h - \alpha q_h$, from (48) it follows that

$$\left(4 \sum_{j=1}^{J-1} \frac{1}{h_j}\right) \alpha = 2b \sum_{j=1}^{J-1} (-1)^j \frac{u_j - u_{j-1}}{h_j} - r,$$

r being the right-hand side of (48). Thus, applying again the stability estimate (39), we have

$$|\alpha| \leq 2 \|f\|_{-h} + \frac{h}{4(J-1)} |r|. \quad (50)$$

From this inequality, (49) and the fact that $2(J-1) \geq J$, the stability estimate (46) follows.

For J even, taking $\varphi_h = q_h$ in (19) and applying (45) we have

$$0 = (b(\tilde{u}_h)_x - f, q_h) + \alpha q_{J-1} = \alpha q_{J-1} + \frac{2}{b} \sum_{j=1}^{J/2} f_{2j-1},$$

so that

$$\alpha = \sum_{j=1}^{J/2} f_{2j-1}. \quad (51)$$

Also, since the equations in (42) are those of the Galerkin method except for the last one, which does not appear in (35) and (36) for J even, we have that for J even (35) and (36) also hold with u_h replaced by \tilde{u}_h . Thus, it follows that

$$\|\tilde{u}_h\| \leq \frac{2}{b} \|f\|_{-h} + |\tilde{u}_{J-1}|. \quad (52)$$

The value of \tilde{u}_{J-1} is then obtained from (48) by replacing \tilde{u}_j by their values as expressed in (35–36), which gives

$$-\left(2b \sum_{j=1}^{J-1} \frac{1}{h_j}\right) \tilde{u}_{J-1} + 4 \sum_{j=1}^{J-2} \left(\frac{1}{h_j} + \frac{1}{h_{j+1}}\right) S_j = r,$$

and, thus,

$$|\tilde{u}_{J-1}| \leq \frac{4}{b} \|f\|_{-h} + \frac{h}{2b(J-1)} |r|, \quad (53)$$

which, together with (52) shows that (46) also holds for J even. \square

Once the stability is proved, we investigate the convergence of the SMS method by considering the basic solution,

$$bu_x = f, \quad u(0) = 0,$$

and the error

$$\tilde{e}_h = \tilde{u}_h - I_h(u),$$

where $I_h(u)$ is the interpolant of u in X_h . We prove different estimates depending on whether

$$\max_{1 \leq j \leq J-1} |h_{j+1} - h_{j-1}| = Ch^2, \quad (54)$$

holds for some constant $C > 0$.

Proposition 2 *There exist a positive constant C such that for $\varepsilon = 0$ the error $e_h = \tilde{u}_h - I_h(u)$ of SMS approximation satisfies the following estimates:*

$$\|\tilde{e}_h\|_{\infty} \leq Ch \|f'\|_{L^1(0,1)}, \quad (55)$$

and, if (54) holds,

$$\|\tilde{e}_h\|_{\infty} \leq Ch^2 (\|f'\|_{\infty} + \|f''\|_{L^1(0,1)}). \quad (56)$$

Proof. We have

$$\frac{b}{2}(\tilde{e}_{j+1} - \tilde{e}_{j-1}) + \left(\alpha - \frac{b}{2}u(1)\right)\delta_{J-1}(j) = \tau_j, \quad j = 1, \dots, J-1, \quad (57)$$

where

$$\tau_j = \int_{x_{j-1}}^{x_{j+1}} f(x) \left(\varphi_j - \frac{1}{2}\right) dx.$$

Since

$$\int_{x_{j-1}}^{x_j} (bI_h(u)_x - f) dx = 0, \quad j = 1, \dots, J-1,$$

so that $(b(\tilde{q}_h)_x, bI_h(u)_x - f)_{L^2(0, x_{J-1})} = 0$, it follows that

$$(b(\tilde{q}_h)_x, b(\tilde{e}_h)_x)_{L^2(0, x_{J-1})} = 0. \quad (58)$$

Thus, applying (46) with f replaced by $\tau = [\tau_1, \dots, \tau_{J-1}]^T$ and r by 0, we have

$$\|\tilde{e}_h\|_\infty \leq \frac{6}{b} \|\tau_h\|_{-h}. \quad (59)$$

Integration by parts reveals

$$\tau_j = - \int_{x_{j-1}}^{x_{j+1}} f'(x) \left(\int_{x_j}^x \left(\frac{1}{2} - \varphi_j \right) dy \right) dx,$$

and, further,

$$\tau_j = f'(x_{j+1}) \frac{h_{j+1}^2}{12} - f'(x_{j-1}) \frac{h_j^2}{12} + \int_{x_{j-1}}^{x_{j+1}} f''(x) \left(\int_{x_j}^x \int_{x_j}^y \left(\frac{1}{2} - \varphi_j \right) dz dy \right) dx.$$

Then, it is easy to check that

$$\|\tau\|_{-h} \leq Ch \|f'\|_{L^1(0,1)}, \quad (60)$$

or

$$\begin{aligned} \|\tau\|_{-h} \leq & \max_{k \leq (J-1)/2} \left(\left| \sum_{j=1}^k f'(x_{2j-1}) \frac{h_{2j}^2 - h_{2j-1}^2}{12} \right| + \left| \sum_{j=k}^{(J-1)/2} f'(x_{2j}) \frac{h_{2j+1}^2 - h_{2j}^2}{12} \right| \right) \\ & + Ch^2 (\|f'\|_{L^\infty(0,1)} + \|f''\|_{L^1(0,1)}). \end{aligned} \quad (61)$$

We notice that from (59) and (60) the estimate (55) follows. On the other hand, if (54) holds, then the right-hand side of (61) is $O(h^2)$, so that (59) and (61) imply (56). \square

Let us finally comment the case $\varepsilon > 0$. In this case, equations (42) should be modified by adding the term

$$\varepsilon \frac{\tilde{u}_j - \tilde{u}_{j+1}}{h_{j+1}} + \varepsilon \frac{\tilde{u}_j - \tilde{u}_{j-1}}{h_j}$$

to the left hand side. Then, the stability estimate (46) holds but with $\|f\|_{-h}$ on the right-hand side replaced by

$$\|f\|_{-h} + 4J\varepsilon \max_{1 \leq j \leq J} \frac{1}{h_j} \|\tilde{u}_h\|_\infty,$$

added to the right-hand side. Thus, we have the same stability estimate (46) with the factor $6/b$ replaced by $12/b$ whenever

$$\varepsilon < \frac{b}{48J} \min_{1 \leq j \leq J} h_j. \quad (62)$$

Finally, with respect to the error, standard asymptotic analysis (see e. g. [36, Theorem 1.4]) shows that the solution u of (3-4) and the basic solution u_0 (solution of (37)) satisfy that

$$\max_{0 \leq x \leq 1} |u(x) - u_0(x) + u_0(1)e^{b(x-1)/\varepsilon}| \leq C\varepsilon,$$

for some $C > 0$ independent of ε . Since $e^{b(x-1)/\varepsilon} < \varepsilon$ for $x < 1 - \varepsilon |\log(\varepsilon)|/b$, then, whenever

$$h_J \geq \frac{\varepsilon |\log(\varepsilon)|}{b}, \quad (63)$$

the bounds (55) and (56) hold if (62) also holds.

Remark 3 As mentioned in the Introduction, in the present paper we are concerned with large Péclet numbers. For this reason and for simplicity, we have not pursued conditions which allow for larger values of ε than (62). Obviously, a more detailed (and lengthy) analysis would allow to obtain more general conditions on ε .

3.2 The multidimensional case

3.2.1 Uniqueness of solutions

In this section we limit ourselves to study the possibility loosing uniqueness in the new method when $\varepsilon = 0$ and how to overcome this in practice. These cases are an indication of when to expect the method to perform poorly for small $\varepsilon > 0$. In the rest of the paper, we denote

$$\hat{\Omega}_h = \Omega \setminus \Omega_h^+.$$

We start by characterizing the solutions of (27–29) when $\varepsilon = 0$. As we now show, they are given by those elements $\tilde{v}_h \in V_h$ satisfying

$$\|L_h(\tilde{v}_h)\|_{L^2(\hat{\Omega}_h)} = 0. \quad (64)$$

To see this, we take $\varphi_h = \tilde{v}_h$ in (27) and get

$$\|L_h(\tilde{v}_h)\|_{L^2(\hat{\Omega}_h)}^2 + a(\tilde{v}_h, z_h) = 0.$$

But taking $\varphi_h = z_h$ in (29) we have

$$a(\tilde{v}_h, z_h) = - \sum_{j \in \mathbb{N}_\delta} t_j z_h(x_j) = 0,$$

where in the last equality we have applied (28). Thus, (64) follows. Conversely, if (64) holds, this implies $L_h(\tilde{v}_h) = 0$ on $\hat{\Omega}_h$. But since we are assuming that $\varepsilon = 0$, we also have that $a(v_h, w_h) = (L_h(v_h), w_h)$ for any $v_h, w_h \in V_h$. Thus, if for a basis function φ_j we have $0 \neq a(\tilde{v}_h, \varphi_j) = (L_h(\tilde{v}_h), \varphi_j)$, it follows that its support cannot be entirely inside $\hat{\Omega}_h$, so that x_j must be in \mathcal{N}_δ . Then taking $z_h = 0$ and $t_j = -a(\tilde{v}_h, \varphi_j)$ we have a solution of (27–29).

We devote the rest of this section to comment on a case that may easily arise in practice where there is a \tilde{v}_h not entirely null in Ω that satisfies (64) (and, hence, the lost of uniqueness in the SMS method when $\varepsilon = 0$). We will also comment on what possible remedies can be applied in practice in these cases. In the rest of the section we assume $c = 0$, that is, $L_h(w_h) = b \cdot \nabla w_h$.

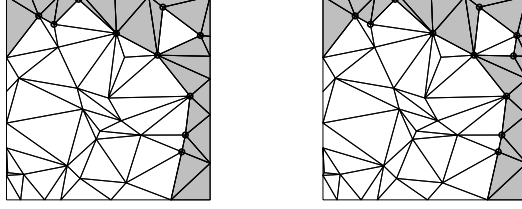


Figure 4: Two triangulations of the unit square with $\hat{\Omega}_h$ of disconnected interior. The set Ω_h^+ for $b = [1, 1]^T$ is shadowed in grey and points of \mathcal{N}_δ are marked with circles.

Consider an example like those in Fig. 4, that is, when the interior set $\hat{\Omega}_h$ of $\hat{\Omega}_h$ is not connected. We may have $\tilde{v}_h \in V_h$ not null in Ω and yet satisfying (64). To see why, take for example the left plot in Fig. 4 and assume that b is constant with strictly positive components for simplicity. Let x_j and x_k be the most downwind vertices of the isolated triangle τ of $\hat{\Omega}_h$. Observe that since their associated basis functions φ_j and φ_k have linearly independent gradients, it is possible to find real values α and β so that $\alpha\varphi_j + \beta\varphi_k \neq 0$ but $b \cdot (\alpha\nabla\varphi_j + \beta\nabla\varphi_k) = 0$. Setting then $\tilde{v}_h = \alpha\varphi_j + \beta\varphi_k$ we have that $\tilde{v}_h \neq 0$ but it satisfies (64). If b is not constant, then it is possible to find \tilde{v}_h such that $\|v_h\|_{L^2(\Omega)} = 1$ but $\|L_h(v_h)\|_{L^2(\hat{\Omega}_h)} \approx \text{diam}(\tau)^2$; there may not be nontrivial solutions of (27–29) but the method may not be very accurate since residuals of size $\text{diam}(\tau)^2$ allow for errors of size $1 = \|v_h\|_{L^2(\Omega)}$. Similar arguments show that this is also the case of the right plot in Fig. 4. These arguments are easily extended to tetrahedra in three-dimensional domains. In Section 3.2.2 we show some other cases where there are nontrivial \tilde{v}_h satisfying (64). We also state general conditions to prevent them.

From the practical point of view, all those conditions are satisfied if the meshes are designed with a strip of elements on Γ_D^{0+} as indicated in Fig. 5. One

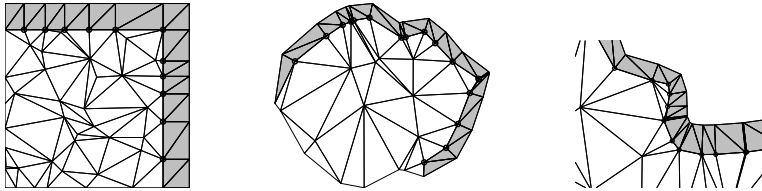


Figure 5: Triangulations with strip of elements on Γ_D^{0+} to prevent isolated components in $\hat{\Omega}_h$. The set Ω_h^+ for $b = [1, 1]^T$ is shadowed in grey.

possible way to form this strip is to take the nodes on the outflow boundary (which we assume partitioned into segments or faces) and displace them along the normal vector to obtain the interior nodes of the strip (see Fig. 6). Then,

sides or faces in the outflow boundary are replicated in the displaced nodes, so that rectangles are obtained in two-dimensional problems and triangular prisms in three-dimensional ones. In the two-dimensional case, the triangulation of the strip is obtained by joining two opposite vertices of the rectangles. In three

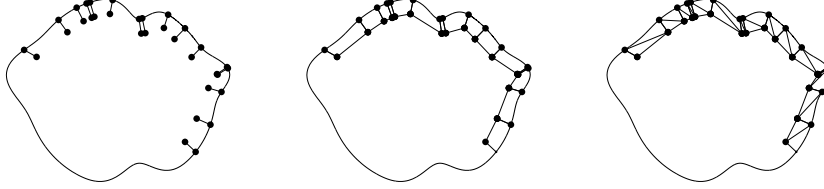


Figure 6: The process to build a strip of elements along Γ_D^{0+} .

dimensions, tetrahedra can be obtained for example by adapting to triangular prisms the so-called Kuhn's triangulation of the cube, [3], [17], [29]. This is a partition of the unit cube into 6 tetrahedra, all of them having the origin and the vertex of coordinates $(1, 1, 1)$, as common vertices. It is a simple exercise to adapt Kuhn's triangulation of the cube to triangular prisms.

We notice, however, that there are times in practice when one cannot choose the grid because it is part of a larger problem, or because it is designed to satisfy some other constraints, etc. In Section 3.2.2, we comment on a different procedure to avoid isolated components in $\hat{\Omega}_h$.

3.2.2 Further cases of lack of uniqueness

We complete the study of the previous section on the cases where there are nontrivial $\tilde{v}_h \in V_h$ satisfying (64). We assume $\varepsilon = 0$ and $c = 0$ here as well. We start by checking that only $\tilde{v}_h = 0$ satisfies (64) when $\hat{\Omega}_h$ is disconnected due to an element upwind of a node interior to B_h , as it was the case discussed in Fig. 3. Let us take that example again. We first notice that since we are assuming that $\varepsilon = 0$, then, (64) imply that \tilde{v}_h is constant along characteristics, and since $\tilde{v}_h = 0$ on Γ_- , it must vanish on the big component of $\hat{\Omega}_h$. This implies that \tilde{v}_h also vanish on the most upwind vertex x_k of the isolated triangle τ . It also vanish on the vertex on the boundary. So it is only on the remaining vertex x_i where it may not vanish. But recall that the triangle τ is upwind of x_i , so that $b \cdot \nabla \varphi_i \neq 0$. Thus, $L_h(\tilde{v}_h) = 0$ on τ implies that $\tilde{v}_h = 0$ on τ .

However, even when $\hat{\Omega}_h$ has a connected interior, there may be nontrivial $\tilde{v}_h \in V_h$ satisfying (64) when there are triangles (resp. tetrahedra) in $\hat{\Omega}_h$, downwind of Ω_h^+ and with one side aligned with the (constant) wind velocity b (resp. one face parallel to b). This is the case of the triangles with one side plotted with a thicker line in the grids in Fig. 7 for $b = [1, 1]^T$. The basis function of the vertices opposite those sides have their gradients orthogonal to b . For example, for the triangle τ marked with a + sign in the center plot of Fig. 7, let x_i be the

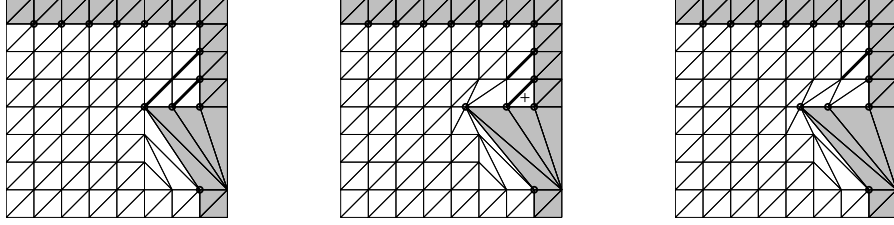


Figure 7: Triangulations of the unit square with triangles in $\hat{\Omega}_h$ downwind of Ω_h^+ and with one side (thicker line) parallel to the wind velocity $b = [1, 1]^T$. The set Ω_h^+ is shadowed in grey.

vertex opposite to the shadowed side on the triangle, and x_j and x_k the other two vertices. Since $b \cdot \nabla \varphi_i = 0$ in τ , and $\varphi_i = 0$ on the rest of $\hat{\Omega}_h$, then $\tilde{v}_h = \varphi_i$ satisfies (64). For the grid in the left plot, we may take $\tilde{v}_h = \alpha \varphi_i + \beta(\varphi_j + \varphi_k)$ for any $\alpha, \beta \in \mathbb{R}$, since $b \cdot \nabla \tilde{v}_h = 0$ in the part of $\hat{\Omega}_h$ downwind Ω_h^+ and \tilde{v}_h is null in the rest of $\hat{\Omega}_h$. As Proposition 3 below shows, there is no nontrivial $\tilde{v}_h \in \Omega$ satisfying (64) for the triangulation on the right-hand side of Fig. 7.

Nevertheless, notice that as it happens with the isolated components in Fig. 4, the cases depicted in Fig. 7 cannot occur if one designs the mesh with a strip of elements along Γ_D^{0+} . However, as commented at the end of Section 3.2.1, there are times in practice when one cannot choose the grid so that cases like those depicted in Fig. 4 or in Fig. 7 may occur. We now comment on the possible remedies to avoid nontrivial solutions of (27–29). For example, one can connect isolated components of $\hat{\Omega}_h$ by enlarging $\hat{\Omega}_h$ with triangles from Ω_h^+ . We have checked in practice that this may leave large portions of Γ_D^{0+} as boundary of $\hat{\Omega}_h$, and this resulted in the presence of spurious oscillations in the computed approximations. A better alternative is to enlarge the grid by refining those elements in Ω_h^+ upwind of the isolated component. In Fig. 8 we show the result of dividing into four similar triangles (red or regular refinement) the two upwind neighbours of the isolated components in Fig. 4 and using longest edge bisection in those triangles that inherit a hanging node. We see that after the refinement process $\hat{\Omega}_h$ is connected. Also, the lack of uniqueness induced by those triangles in $\hat{\Omega}_h$ with a side parallel to b downwind of Ω_h^+ can be prevented by red-refining their upwind triangles in Ω_h^+ , as it can be seen in Fig. 9, where no side parallel to the wind velocity b is now downwind of Ω_h^+ .

The following result states general conditions guaranteeing that (64) implies $\tilde{v}_h = 0$. Consider the set of points that are not downwind of Ω_h^+ , that is,

$$d(\hat{\Omega}_h) = \{x \in \hat{\Omega}_h \mid \{x - tb \mid t > 0\} \cap \Omega_h^+ = \emptyset\}.$$

Proposition 3 *Let b be constant and $c = 0$. Then if either $d(\hat{\Omega}_h) = \hat{\Omega}_h$ or for*

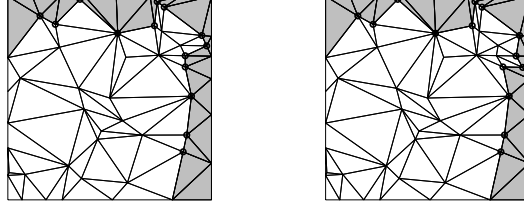


Figure 8: The triangulations in Fig. 4 after regular refinement of upwind triangles closest to isolated components. The new set Ω_h^+ for $b = [1, 1]^T$ is shadowed in grey and points of the new \mathcal{N}_δ are marked with circles.

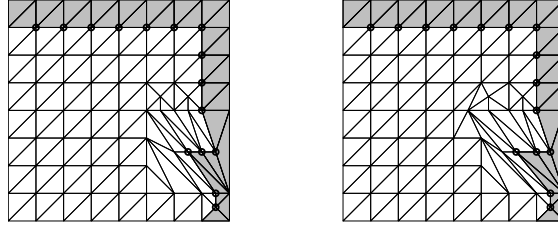


Figure 9: The triangulations in Fig. 7 after regular refinement of triangles in Ω_h^+ upwind of $\hat{\Omega}_h$. The set Ω_h^+ for $b = [1, 1]^T$ is shadowed in grey and points of the new \mathcal{N}_δ are marked with circles.

any $x \in \mathring{\hat{\Omega}}_h \setminus \overline{d(\Omega_h)}$ there is a path in $\mathring{\hat{\Omega}}_h$ from x to a point $y \in d(\Omega_h)$ through elements with no edge or face parallel to b , then the only element $\tilde{v}_h \in V_h$ satisfying (64) is $\tilde{v}_h = 0$.

Proof. If $\tilde{v}_h \in V_h$ satisfies (64), then $\tilde{v}_h = 0$ on $d(\hat{\Omega}_h)$, since any \tilde{v}_h satisfying (64) is constant along the characteristics $x + tb$ which, eventually intersect Γ^- where $\tilde{v}_h = 0$. If $d(\hat{\Omega}_h) = \mathring{\hat{\Omega}}_h$, then \tilde{v}_h can only be nonzero on Ω_h^+ . But elements on Ω_h^+ have vertices either on Γ_D^{0+} where $\tilde{v}_h = 0$ or on $\hat{\Omega}_h$. Thus, \tilde{v}_h must be zero on every element in Ω_h^+ .

Suppose now that, $d(\hat{\Omega}_h) \neq \mathring{\hat{\Omega}}_h$. Then, for $x \in \mathring{\hat{\Omega}}_h \setminus \overline{d(\hat{\Omega}_h)}$, let γ be the path in $\mathring{\hat{\Omega}}_h$ connecting x to a point $y \in d(\hat{\Omega}_h)$, not intersecting any element with a side or face parallel to b . There is no loss of generality in assuming the path to be a polygonal, and except maybe from the first and last segments, the remaining segments joint the barycenters or arithmetic means of the vertices of the elements it intersects. There will be a first element τ of those intersected by γ which is not entirely inside $\mathring{\hat{\Omega}}_h \setminus \overline{d(\hat{\Omega}_h)}$. Since τ has no edge or face parallel to b , then its interior $\hat{\tau}$ is not entirely contained in $\mathring{\hat{\Omega}}_h \setminus \overline{d(\hat{\Omega}_h)}$, and thus, \tilde{v}_h must vanish on τ . But then, the previous element is in a similar situation, with \tilde{v}_h vanishing on the side or face in common with τ and this side or face not being

parallel to b , so that \tilde{v}_h is zero in that element too. Repeating the argument we conclude that \tilde{v}_h vanish in x . \square

Finally, for those situations in practice where one has to work with a mesh without a strip of elements along Γ_D^{0+} , we now study how to make robust the technique of red-refining adequate triangles in Ω_h^+ . We first notice that it is not difficult to design examples where red-refining even *all* triangles in Ω_h^+ does not make $\mathring{\Omega}_h$ connected. However, we now argue that two red-refinements are enough to connect any isolated component. This is done as in the proof of Proposition 3 by considering a polygonal path in Ω joining the isolated component with with another component upwind of it. The segments of the path may be assumed to join barycenters (resp. arithmetic means of the vertices) of triangles with a common side (resp. tetrahedra with a common face). Consider a refinement strategy where all sides or edges are bisected, and apply it to all elements in Ω_h^+ intersecting the path. It is not difficult to analyze all possible cases, the worst cases being those where all vertices are in Γ_D^{0+} and all sides (resp. faces) except those two intersecting the path are also on Γ_D^{0+} . After two refinements the elements in Ω_h^+ are restricted to be in the area or volume induced by the new vertices of the second refinement closest to the initial vertices, as we show in Fig. 10. Then, in the two-dimensional case, the original path is completely embedded in $\mathring{\Omega}_h$, and, in the three-dimensional case, it is on the border of $\mathring{\Omega}_h$, so that a small change moves it into $\mathring{\Omega}_h$.

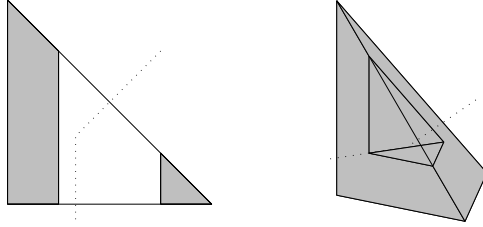


Figure 10: Two and three-dimensional elements showing shadowed in grey the part where Ω_h^+ is restricted to be after two refinements where all sides and edges are bisected. Dotted lines are path entering and leaving the element through the only sides and faces not on the boundary of Ω and passing through the barycenter.

Let us mention that in the case of tetrahedra, the so-called regular refinement is not unique [3], and that the arguments above also apply if the refinement is done by successive bisection of the six edges of the tetrahedron using, for example, the technique in [1], or, in the case of triangles, three applications of longest-edge bisection to the three sides of a triangle.

4 Numerical Experiments

In this section we solve (1–2) on different domains Ω and with different forcing terms and vector fields b . In all cases we take $c = 0$. We used Matlab 7.13.0 and the backslash command to solve linear systems. Also, for the SUPG method, we take the streamline diffusion parameter as suggested in formulae (5-7) in [26], which we reproduce here for the convenience of the reader. More precisely, in the SUPG method test functions on element τ are of the form $\varphi_h + \delta_\tau b \cdot \nabla \varphi_h$, where δ_τ is given by

$$\delta_\tau = \frac{\text{diam}(\tau, b)}{2|b|}, \quad \text{if } \text{Pe}_\tau > 1, \quad (65)$$

$$\delta_\tau = \frac{\text{diam}(\tau, b)^2}{4\varepsilon}, \quad \text{if } \text{Pe}_\tau \leq 1, \quad (66)$$

where $\text{Pe}_\tau = \frac{|b|\text{diam}(\tau, b)}{2\varepsilon}$, and, if $\varphi_1, \dots, \varphi_{d+1}$ are the basis functions in element τ (taking value 1 on one of the vertices and 0 on the rest of them) then

$$\text{diam}(\tau, b) = \frac{2|b|}{|b \cdot \nabla \varphi_1| + \dots + |b \cdot \nabla \varphi_{d+1}|}.$$

Here $|b|$ stands for the euclidean norm of the vector field b . If b is not constant, it is evaluated at the barycenter of element τ . The Matlab codes used in this section are available from the author on request (check also the url address http://personal.us.es/bga/bga_files/software_bga.html). Excluded are the codes corresponding to Example 7 which is subject of current research.

Example 1 *Simulation of Shishkin grids.* Since the SMS method was conceived as a simulation of a Shishkin grid, we now check how well it does it. We take $\Omega = (0, 1)^2$, $b = [2, 3]^T$, Dirichlet homogeneous boundary conditions and the forcing term f such that the solution is

$$u(x, y) = (x - e^{2(x-1)/\varepsilon})(y^2 - e^{3(y-1)/\varepsilon}).$$

This example is taken from Example 5.2 in [25], but in our case $c = 0$. On the one hand, we solve this problem with the SUPG method on Shishkin meshes with $J = 2N$ subdivision in each coordinate direction. They are formed as tensor products of one-dimensional Shishkin meshes, with values $\sigma_x = 2\varepsilon \log(N)$ and $\sigma_y = (3/2)\varepsilon \log(J)$ on the x and y directions, respectively. On the other hand, we take the coarse part of the Shishkin mesh, which is a triangulation of

$$\Omega_\sigma = [0, 1 - \sigma_x] \times [0, 1 - \sigma_y], \quad (67)$$

with N subdivisions in each coordinate direction, and apply the SMS method (both Galerkin-based and SUPG based). For $N = 5, 10, 20, \dots, 320$, we compute the numerical approximations and measure both the computing time and the L^∞ errors in the interior points of the coarse part of the Shishkin grid (points which are shared by the three methods) for $\varepsilon = 10^{-4}$ and $\varepsilon = 10^{-8}$. Results

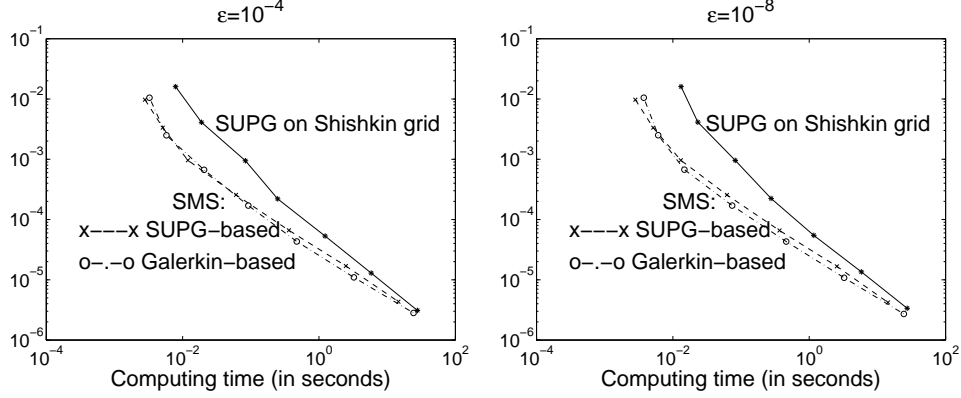


Figure 11: Relative efficiency of SMS and SUPG methods in Example 1.

are shown in Fig. 11. Looking at the errors, and for both values of ε , we notice that the three methods commit roughly the same errors, being in this example those of the SUPG-based SMS method slightly worse in general. In terms of computational efficiency, though, both SMS methods are roughly equally efficient, and markedly better than the SUPG method on Shishkin grids, since although the three methods commit roughly the same errors, the SMS methods compute the approximations between 4 and 2 times faster than the SUPG on the Shishkin grid (only for $N = 320$, the SMS methods were only 1.2 times faster than the SUPG method). In the next example, we further comment on computational costs and the structure of the linear systems to be solved to obtain the different approximations.

Example 2 *Comparisons on the same grid.* In the previous example, it may be considered unfair to compare the new methods on an $N \times N$ coarse grid with the SUPG on a $2N \times 2N$ grid, since this is bound to be more expensive. In the present example we apply the methods on the same grids (uniform with diagonals running Southwest-Northeast). The convection-problem is the same as in the previous example, and, as before, L^∞ errors are measured in interior mesh points. The SUPG method in this example gave very poor results, with errors above 10^{-1} . For this reason, and following suggestions in [30], we programmed it with some crosswind diffusion. More precisely, if in the SUPG method test functions on element τ are of the form $\varphi_h + \delta_\tau b \cdot \nabla \varphi_h$, where δ_τ is the stabilization parameter, we used $\varphi_h + \delta_\tau (b \cdot \nabla \varphi_h + \delta_c \partial_x \varphi)$ where the value of δ_c was set by trial and error to obtain the smallest errors. These values were $\delta_c = 0.7701, 0.8783$ and 0.9365 , for $N = 10, 20$ and 40 subdivisions in each coordinate direction. For similar reasons, the value of δ_τ in formulae (5-7) in [26], was multiplied by 1.57, 1.615 and 1.64 for the above-mentioned number of subdivisions, respectively.

The results can be seen in Fig. 12. Even though the SMS methods can be up to twice as costly as the SUPG on the same grid, the errors are, however, between 13 and 60 times smaller (SUPG-based SMS) and 26 and 130 (Galerkin-based SMS), so that the SMS method is computationally much more efficient.

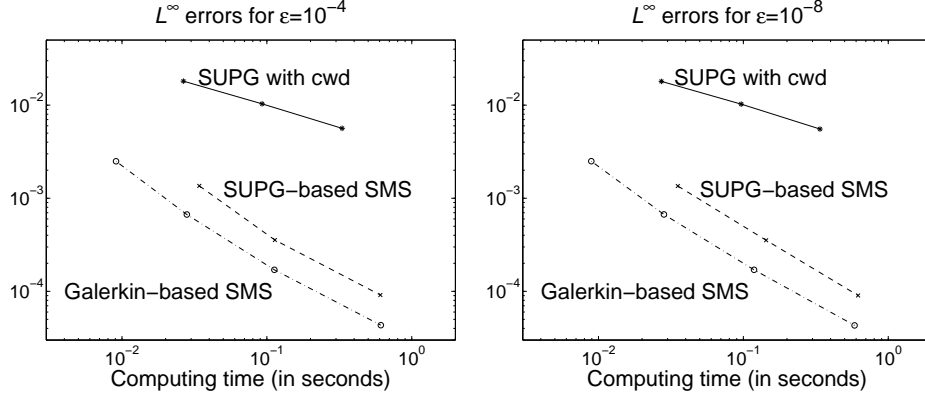


Figure 12: Relative efficiency of SMS and SUPG (with crosswind diffusion) methods in Example 2.

Let us comment here on the computational cost of the methods. Recall that the SMS approximation \tilde{u}_h is obtained (together with the Lagrange multipliers z_h and the values $t_j, j \in \mathbb{N}_\delta$ as the solution of the optimality conditions (24-26). Let $\varphi_1, \dots, \varphi_n$ be the nodal basis of V_h (each φ_i takes value 1 on one single node of the triangulation and 0 on the rest of them), and let A and S be the $n \times n$ matrices with entries

$$a_{i,j} = a(\varphi_i, \varphi_j), \quad s_{i,j} = (L(\varphi_i), L(\varphi_j))_{L^2(\Omega \setminus \Omega_h^+)}, \quad 1 \leq i, j \leq n,$$

(or $a_{i,j} = a_h(\varphi_i, \varphi_j)$ in the case of the SUPG method) respectively, and let E be the $n \times m$ matrix whose columns are those of the $n \times n$ identity matrix corresponding to the indexes in \mathbb{N}_δ . Notice that we may assume $m \approx \rho n^{(d-1)/d}$ for some $\rho > 0$, (d being the dimension of the euclidean space where the domain Ω is). Observe also that A , S , and E are typically sparse matrices. The nodal values of \tilde{u}_h , the values $t_j, j \in \mathbb{N}_\delta$ and the nodal values of z_h are then obtained by solving a linear system whose coefficient matrix is

$$M = \begin{bmatrix} S & 0 & -A^T \\ 0 & 0 & -E^T \\ A & E & 0 \end{bmatrix}. \quad (68)$$

This must be compared with the SUPG method where the coefficient matrix is A , that is, a system of order n , whereas the SMS method is of order $2n + \rho n^{(d-1)/d}$

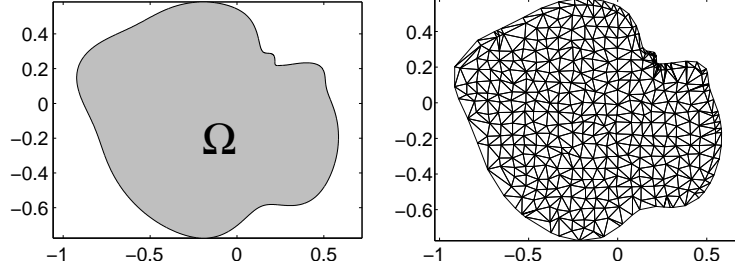


Figure 13: The domain of Example 3 (left) and a random grid (right).

However, as Fig. 12 shows, the errors in the SMS method are so small that greatly compensate for the large computational cost. Also, as Fig. 11 shows, the comparison is favourable with the Galerkin method on Shishkin meshes, where systems of order $2^d n$ have to be solved.

On the other hand notice that the change of variables $z_h = -z_h$, changes $-A^T$ and $-E^T$ in M to A^T and E^T , respectively, so that the coefficient matrix in the SMS method is symmetric. This allows to use methods and software for sparse symmetric indefinite matrices which are generally faster than methods for general sparse matrices (like those in the SUPG or Galerkin methods). A study of the performance of the direct methods available today for sparse symmetric matrices can be found in [20], where the codes MA57 [12] and PARDISO, [40], [41], appear as best performers. Note however that only serial versions were tried in [20] and that this is an area of fast development. As for iterative methods, the fact that SMS approximation can be found by solving a symmetric system allows the use of three term recurrence methods like the MINRES method of Paige and Saunders [34] (see e. g. [5], [11], [13], [21], [42] and the references cited therein for information on preconditioning this kind of systems). We remark that for the systems in the SMS method, Matlab's backslash command seems to take no advantage of the symmetry of the systems, and, thus, no advantage has resulted from that symmetry in the experiments reported in the present paper.

Example 3 *Irregular grids on curved domains.* We now consider domains where it may not be easy to set up a Shishkin grid. In particular, we consider the domain Ω enclosed by the following curve:

$$\gamma(t) = \frac{26 + 7(1 - \sin^9(2t))}{40(2 + \sigma)\sqrt{2}} \begin{bmatrix} 1 & -1 \\ 1 & 1 \end{bmatrix} \begin{bmatrix} 2 \cos(t) - \sigma \cos(2t) \\ 2 \sin(t) - \sigma \sin(2t) \end{bmatrix}, \quad t \in [0, 2\pi],$$

where $\sigma = 0.9$. The curve was created by tilting 45 degrees a centered trochoid and altering its size in order to have the shape depicted in Fig. 13. In this domain we consider problem (1-2), with $b = [2, 3]^T$ and constant forcing term $f = 1$, with Dirichlet homogeneous boundary conditions.

We study the behaviour of SMS methods on irregular grids, built as follows. For a given positive integer N , we consider Delaunay triangulations with $(N+1)^2$

points in $\overline{\Omega}$, where $4N$ of them are randomly distributed on $\partial\Omega$. If N_o of these are on Γ_D^{0+} , then, we built the strip of elements along Γ_D^{0+} as indicated in Fig. 5. The remaining points are generated by first fitting a uniform grid inside Ω and the outflow strip, its diameter h in the x and y direction being the value for which the number of points is the closest to $(N - 1)^2 - N_o$, and then by displacing each point randomly on the x and y directions with a uniform distribution on $[-h/3, h/3]$. We show one of such grids for $N = 20$ in Fig. 13.

For $N = 40$, we generated 200 random grids and on each of them we computed the SUPG and SMS approximations and their L^2 error in the convective derivative in $\hat{\Omega}_h$, that is

$$\|b \cdot \nabla w_h - 1\|_{L^2(\hat{\Omega}_h)},$$

w_h being each of the three approximations. The errors on the 200 grids for $\varepsilon = 10^{-4}$ and $\varepsilon = 10^{-8}$ are depicted in Fig. 14 (marked differently for each method). The results have been reordered so that those of the SUPG method appear in

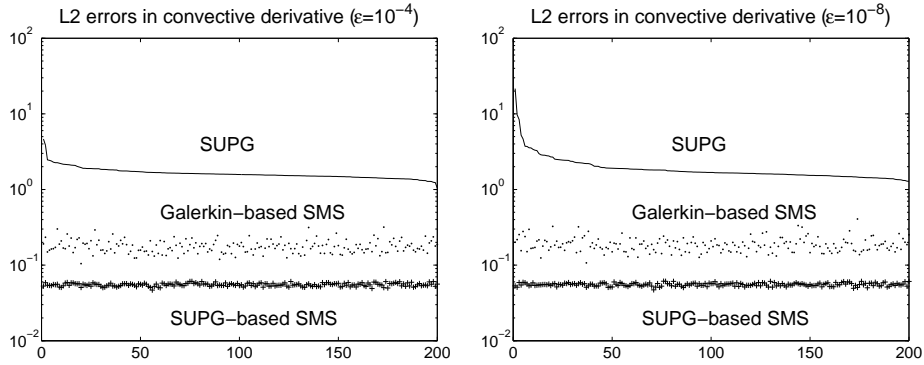


Figure 14: Errors in convective derivative on random grids for $\varepsilon = 10^{-4}$ (left) and 10^{-8} (right).

descending order. We see that the SMS methods clearly improve the errors of the SUPG method, specially so in the case of the SUPG-based SMS method. Computing the ratios of the error of the SUPG method and each of the SMS methods and taking the arithmetic mean, the resulting values for the Galerkin-based and SUPG-based SMS methods are, respectively, 9.64 and 30.19 for $\varepsilon = 10^{-4}$ and 11.42 and 37.69 for $\varepsilon = 10^{-8}$. That is, the SMS methods commit errors that are, on average, between 4 and 33 times smaller than those of the SUPG method. For $\varepsilon = 10^{-8}$ we repeated these computations for growing values of N , and the ratios between the errors of the SUPG method and the SMS method grew with N . For example, for $N = 320$, these were 46.93 and 380.41 for the Galerkin-based and SUPG-based SMS methods, respectively.

In Fig. 15, where we compare the the SUPG-based SMS approximation that produced the largest error (left) with that of the SUPG method that pro-

duced the smallest error (right). We notice the typical oscillations of the SUPG

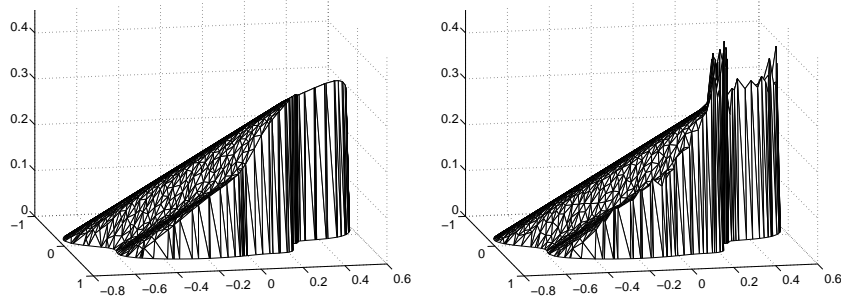


Figure 15: The worst case of the SUPG-based SMS method (left) and the best case of the SUPG method (right).

method, which are located only near the outflow boundary but are of considerable amplitude. The SMS method, on the contrary presents no oscillations. Similarly, in Fig. 16 we show the Galerkin-based SMS approximations that produced the largest and smallest errors (left and right, respectively). Both of them compare very favourably with the best case of the SUPG method in Fig. 15. We notice however that some small amplitude oscillations can be observed in

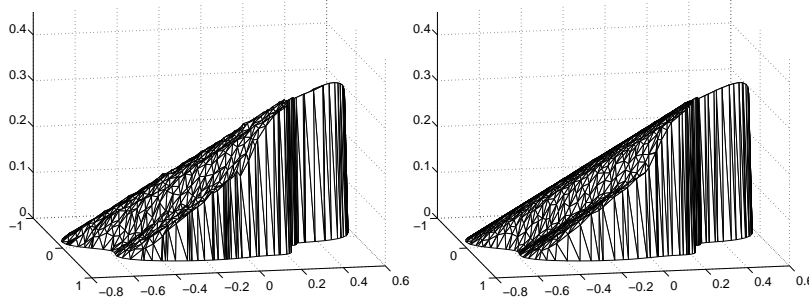


Figure 16: The worst and best cases of the Galerkin-based SMS method.

the worst case of the Galerkin-based SMS method. We believe that these are due to the irregularity of the grid, since making the grids less irregular (i.e., smaller random perturbations) diminishes these small oscillations in the worst case, whereas making them more irregular increases them. It is to be remarked, though, that the irregularity of the grid does not affect the SUPG-based SMS method. Some results explaining the degradation of performance of the Galerkin method on irregular grids can be found in [10] and [44]. Also, further numerical experiments with the SMS method on irregular grids can be found in [19].

Example 4 *Parabolic Layers.* We solve (1) on $\Omega = (0, 1)^2$, with $\varepsilon = 10^{-8}$, $b = [1, 0]^T$ and f constant equal to 1 with Dirichlet homogeneous boundary conditions. This is a well-known test case (see e.g., [26]). The solution presents an exponential layer at the outflow boundary at $x = 1$ and parabolic or characteristic layers along $y = 0$ and $y = 1$ (see e. g., [36] for a precise definition of these concepts). In Fig. 17 we show the SUPG and SMS approximations on a 20×20 regular grid with Southwest-Northeast diagonals. We notice that whereas the SUPG approximation suffers from the typical oscillations along the characteristic layers, the SMS approximation is free of oscillations, both in the exponential layer at $x = 1$ and along the characteristic layers.

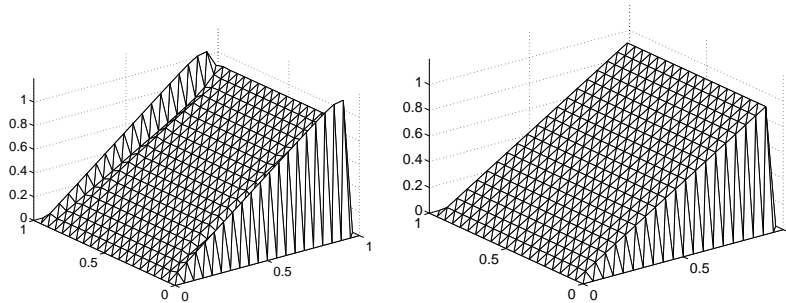


Figure 17: The SUPG (left) and the SMS approximation in Example 4.

In [26], several techniques to reduce the oscillations of the SUPG method are tested. In this example, for approximations w_h computed on a regular 64×64 grid, the following quantities

$$\text{osc} := \max_{y \in \{1/64, \dots, 63/64\}} \{w_h(0.5, y) - w_h(0.5, 0.5)\}, \quad (69)$$

$$\text{smear} := \max_{y \in \{1/64, \dots, 63/64\}} \{w_h(0.5, 0.5) - w_h(0.5, y)\}, \quad (70)$$

are computed in [26] as a measure of the oscillations and the smearing along the characteristic layers, desirable values being, respectively, between 0 and 10^{-3} and between 0 and 10^{-4} . The value of osc and smear for all the methods tested in [26] except one was always larger than 10^{-4} . The values in the case of SMS methods were below 10^{-14} . The value of osc in the SUPG method in our tests coincided with that in [26], 0.134 (no value of smear was given in [26]).

Similar striking contrast between methods tested in [26] and the SMS methods can be found in the experiments on randomly-generated grids for this example in [19].

Example 5 *Interior layers.* This example is also taken from [26]. We solve (1) on $\Omega = (0, 1)^2$, with $\varepsilon = 10^{-8}$, $b = [\cos(-\pi/3), \sin(-\pi/3)]^T$, $f = 0$, and $u = g$

on $\partial\Omega$ where

$$g(x, y) = \begin{cases} 0, & \text{if } x = 1 \text{ or } y \leq 0.7 \\ 1, & \text{otherwise.} \end{cases}$$

The solution possesses an interior layer starting at $x = 0$ and $y = 0.7$, and an exponential layer on $x = 1$ and on the right part of $y = 0$. For SMS methods, the only way we have conceived so far to deal with interior layers is to treat them as parabolic layers. For this to be possible, the grid has to include the characteristic curve that starts at the discontinuity of the boundary data (or a polygonal approximation to it in case of curved characteristics). We will refer to this characteristic curve as the *layer characteristic*. For grids as those depicted on the left of Fig. 18, where the layer characteristic is not part of the grid, one

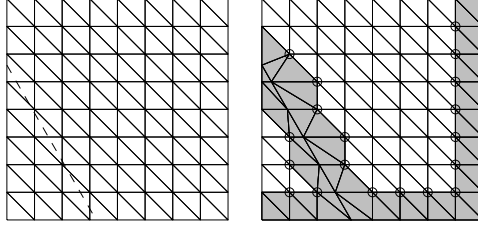


Figure 18: Left, a 8×8 uniform grid in Example 5, with the characteristic curve of the internal layer (dashed line). Right, the grid on the left but moving to the internal layer characteristic its closest points on the grid.

possibility to make it part of it is to move to the layer characteristic its closest points in the grid, as we show on the right plot in Fig. 18 (see also the next example for an alternative). Once this is done, one has to set the value of the solution along the layer characteristic as part of Dirichlet boundary conditions. To do this, we integrate the reduced problem (i.e., (1-2) when $\varepsilon = 0$) along the layer characteristic. In the present case, this procedure gives $u = 0.5$ on the layer characteristic.

With these provisions, we compute the approximations of the SUPG method SMS methods on a 16×16 grid. The results are shown in Fig. 19 (the SMS approximations were identical and only the Galerkin-based one is shown). As before, the SMS method produces an approximation with no oscillations, in sharp contrast with the SUPG method. Comparison with the methods tested in [26] can be found in [19], with results very similar to those of the previous example.

Example 6 Hemker problem. Here, $\Omega = (-3, 9) \times (-3, 3) \setminus \{x^2 + y^2 \leq 1\}$, $b = [1, 0]^T$ and $f = 0$. The boundary conditions are

$$u(x, y) = \begin{cases} 0 & \text{if } x = -3, \\ 1, & \text{if } x^2 + y^2 = 1, \\ \varepsilon \nabla u \cdot n = 0, & \text{elsewhere.} \end{cases} \quad (71)$$

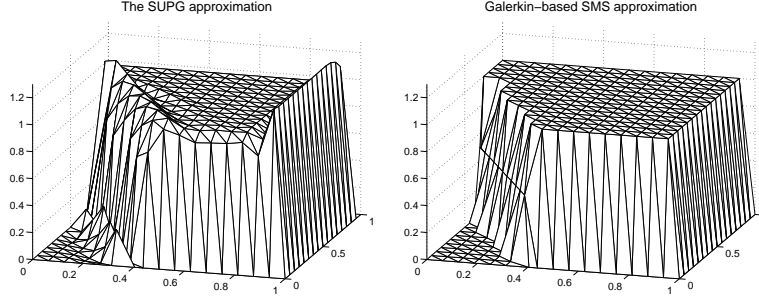


Figure 19: The SUPG and SMS (Galerkin-based) approximations on a 20×20 regular grid in Example 5.

This problem, which was originally proposed in [22], models a hot column (the unit circle) with normalized temperature equal to 1, and the heat being transported in the direction of the wind velocity b . Thus, a boundary layer appears in the upwind part of the unit circumference from the lowest to highest point, and two internal layers start from these two points and spread in the direction of b . Notice also that part of the boundary is curved, a feature which is often encountered in applications.

We are going to present results corresponding to $\varepsilon = 10^{-8}$ on the grid shown in Fig. 20, which has 932 triangles and 531 nodes. The interior layer

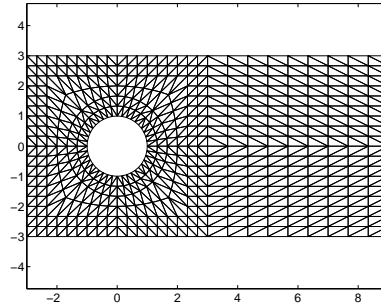


Figure 20: The grid in Example 6.

characteristics are not part of this grid, as it can be seen in Fig. 21, where we show one of the layer characteristic in a dashed line. We have seen in the previous example that interior layers are treated in the SMS method in the same way as characteristic boundary layers, so that they must be part of the grid. Rather than moving grid points to the layer as we did in the previous example, in the present one we will enlarge the grid with more triangles and vertices so that the layer characteristic is part of it (an example is shown in Fig. 21). This may be useful in those cases in practice where, as commented at the end of

Section 3.2.1 one does not have the freedom to choose or move the grid points.

Thus, we now describe a general technique to enlarge grids in order to include an inner layer characteristic. For simplicity we describe it for two-dimensional problems. Let γ be the inner layer characteristic. We assume that the mesh is sufficiently fine so that γ can be well approximated by a straight segment in the interior of every triangle τ it intersects. Let τ be such a triangle. If γ passes through a vertex v , then the τ is bisected by γ into two triangles. These two triangles are included in the enlarged triangulation. Otherwise, γ intersects two sides, and the element τ is divided by γ into a triangle and a quadrilateral (see an example in Fig. 22) which in turn is divided into four triangles. We remark

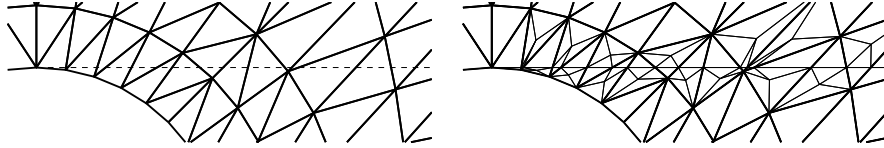


Figure 21: Left. Detail on the grid in Fig. 20 showing one of the inner layer characteristic (dashed line). Right: the same grid enlarged with more triangles and nodes to include the layer characteristic. New sides are plotted with thinner lines.

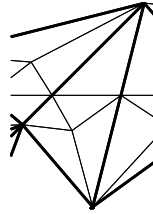


Figure 22: Detail of the enlarged grid in Fig. 21 showing a triangle of the original grid being divided by the layer characteristic in a triangle and a quadrilateral, which we divide into triangles by joining the vertices with their arithmetic mean.

that it is easy to conceive better strategies to enlarge the triangulation in order to include the layer characteristic (techniques that avoid long-shaped triangles, for example), but we have chosen this one due to its simplicity. Nevertheless, as the experiments below show, its simplicity does not prevent it from obtaining excellent results.

Fig. 23 shows the SUPG and the SMS approximations (Galerkin-based). Oscillations can be clearly seen in the SUPG approximation, but they are absent in the SMS approximation. This can be better observed in the bottom plots, where a different point of view is taken. Following [2], we measure the undershoots of an approximation w_h as $\min \{w_h\}$ and the overshoots as $\max \{w_h - 1\}$. The

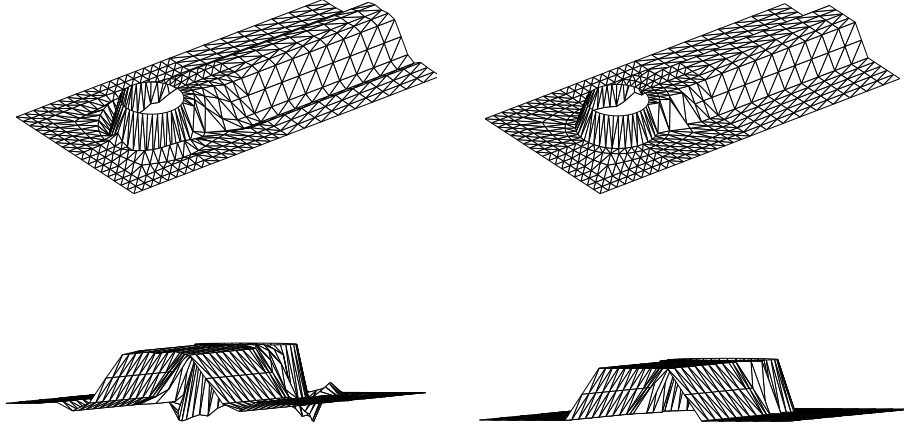


Figure 23: The SUPG approximation (left) and the Galerkin-based SMS approximation (right) on the grid depicted in Fig.20. A different point of view is taken on the bottom plots.

over and undershoots for the SUPG method were 0.04 and -0.52 , whereas for both SMS methods the overshoots were smaller than 10^{-15} , and the undershoots were 0. Similar results were obtained by doubling and multiplying by four the number of subdivisions in each coordinate direction. The results of the SMS method compare very favourably not only with the SUPG method, but with most of the methods tested in [2], which had values very similar to those of the SUPG method. They also compare very favourably with results in [18], where LPS methods present oscillations of about 5% of the jump, whereas the SMS methods of less than $10^{-13}\%$.

In [19], the previous experiment is repeated with the vector field b changed to $b = [\cos(\theta), \sin(\theta)]^T$, for 100 equidistant values of θ between $(0, \pi/4]$, with results similar to those shown here for all cases except four, where, in order to get over and undershoots of order 10^{-12} it was also necessary for nodes $O(h_{\min}^2)$ away from interior layers to be allowed to move (see [19] for details).

Example 7 *Double-glazing test problem* [13]. This is an example where the vector field b has vortices. The domain is $\Omega = (-1, 1)^2$, $f = 0$, and the wind velocity is $[y(1-x^2), -x(1-y^2)]$, so that the characteristic curves are the closed curves given by

$$\{(x, y) \mid (1-x^2)(1-y^2) = \text{constant}\},$$

(See Fig. 24). The Dirichlet boundary conditions are $u = 1$ on $x = 1$ and $u = 0$ otherwise, so that there are discontinuities in the data at corners in

$x = 1$, $y = \pm 1$. These discontinuities give rise to parabolic boundary layers which, according to [13], have a structure difficult to compute by asymptotic techniques.

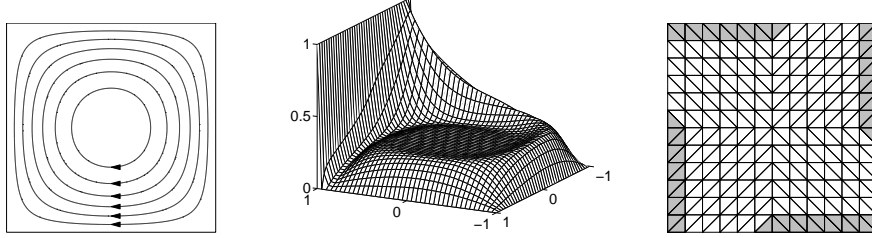


Figure 24: Left: The streamlines in Example 7. Center: the solution in Example 7 for $\varepsilon = 0.005$. Right: A regular mesh, with the set Ω_h^+ shadowed in grey and points of \mathcal{N}_δ are marked with circles.

Notice that the hypotheses stated at the beginning of Section 2.2 ($b(x) \neq 0$ and all characteristics entering and leaving the domain in finite time) do not apply to vector fields with vortices or closed integral curves. Nevertheless, as we now show, the results of the SMS method in the present example are as good as in the previous ones, even though part of the analysis in Section 3.2 does not apply to the present case.

Observe that since the four sides of the boundary are themselves characteristic curves, we have $\Gamma_D^{0+} = \partial\Omega$, so that building Ω_h^+ as described in Section 2.2 results in Ω_h^+ being composed by all elements touching the boundary. In this case the SMS method produces an approximation equal to 0 on all nodes except on those on $x = 1$, where it takes value one, and this is only correct for $\varepsilon = 0$. For $\varepsilon > 0$, better results are obtained with the SMS method if, as we show in Fig. 24, the set Ω_h^+ is shrunk so as to correspond to that of a slightly smaller rectangular domain, that is, elements are included in Ω_h^+ if they intersect the outflow boundary of $(-1 + \delta, 1 - \delta)^2$ for a small $\delta > 0$ (other possibilities to obtain better results with vector fields with vortices will be reported in future works). With this selection of Ω_h^+ , the results of the Galerkin-based SMS method for $\varepsilon = 10^{-4}$ can be seen in Fig. 25. Also shown in Fig. 25 is the SUPG approximation, where we can observe oscillations along the characteristic layers, especially at $x = 1$ and $y = -1$. In sharp contrast, the SMS method produces a nonnegative approximation. For this value of ε , in order to obtain nonnegative approximations on a regular $N \times N$ mesh with the SUPG method one must take $N \geq 144$, and $N \geq 240$ with the Galerkin method; for $\varepsilon = 10^{-5}$, this is achieved for $N \geq 682$ and $N \geq 800$ with the SUPG and Galerkin methods respectively, and for $\varepsilon = 10^{-6}$, neither method was able to obtain nonnegative approximations with all the meshes we tried up to $N = 1800$. In sharp contrast, with the SMS method, both Galerkin-based and SUPG-based, nonnegative approxi-

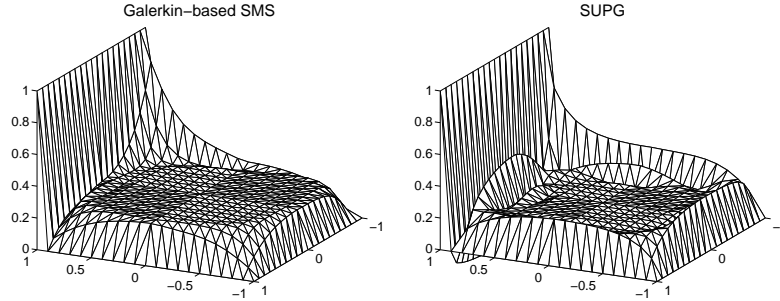


Figure 25: The Galerkin based SMS method (left) and the SUPG method on a 20×20 regular grid in Example 7 for $\varepsilon = 10^{-4}$.

mations were obtained for $N \geq 8$ and ε as small as 10^{-14} .

5 Concluding remarks

A novel stabilization technique for convection-diffusion problems has been introduced, tested and partially analyzed. It can be applied to most existing methods based on conforming piecewise linear finite elements. It consists of, first, adding extra values to the residual of the method on nodes next to the outflow and characteristic boundaries. The resulting equations are taken as a restriction on a least-squares problem on the elementwise residuals of the convection-diffusion operator, where elements next to the outflow and characteristic boundaries (and internal layers) are left out.

The method has been tried in a series of standard and nonstandard tests, and results seem to suggest it performs manifestly better than a good deal of the methods of choice today. The tests include exponential and characteristic layers, and even irregular grids on domains with nontrivial geometries. This is so in spite of the method being initially conceived as a simulation on the coarse part of a Shishkin mesh. The tests also include interior layers and convection with vortices, with similarly outstanding results, although numerical experiments in the present paper and in [19] suggest that further research may be needed on these topics.

Besides the practical performance shown in tests, it is to be remarked the lack of parameters in the method (in markedly contrast with most of existing stabilized methods today). Subject of future research will be extending the method to finite elements of higher degree, as well as the possible changes when the mesh Péclet number tends to one.

Acknowledgements. The author wish to thank Prof. Martin Stynes for advice and helpful discussions in the research summarized in this paper.

References

- [1] D. N. Arnold, A. Mukherjee & L. Pouly, Locally adapted tetrahedral meshes using bisection, *SIAM J. Sci. Comput.*, 22 (2000), 431–448.
- [2] M. Augustin, A. Caiazzo, A. Fiebach, J. Fuhrmann, V. John, A. Linke & R. Umla, An assessment of discretizations for convection-dominated convection-diffusion equations, *Comput. Methods Appl. Mech. Engrg.*, 200 (2011), 3395–3409.
- [3] J. Bey, Simplicial grid refinement: on Freudenthals algorithm and the optimal number of congruence classes, *Numer. Math.*, 85 (2000), 1–29.
- [4] R. Becker & M. Braack, A finite element pressure gradient stabilization for the Stokes equations based on local projections, *Calcolo*, 38 (2001), 173–199.
- [5] M. Benzi, G. H. Golub & J. Liesen, Numerical solution of saddle point problems, *Acta Numer.*, 14 (2005), 1–137.
- [6] M. Braack & E. Burman, Local projection stabilization for the Oseen problem and its interpretation as a variational multiscale method, *SIAM J. Numer. Anal.*, 43 (2006), 2544–2566.
- [7] A. N. Brooks & T. J. R. Hughes, Streamline upwind/Petrov-Galerkin formulations for convection dominated flows with particular emphasis on the incompressible Navier-Stokes equations, *Comput. Methods Appl. Mech. Eng.*, 32 (1982), 199–259.
- [8] E. Burman, A unified analysis for conforming and nonconforming stabilized finite element methods using interior penalty, *SIAM J. Numer. Anal.*, 43 (2005), 2012–2033.
- [9] E. Burman & P. Hansbo, Edge stabilization for Galerkin approximations of convection-diffusion-reaction problems, *Comput. Methods Appl. Mech. Eng.*, 193 (2004), 1437–1453.
- [10] L. Chen & J. Xu, Stability and accuracy of adapted finite element methods for singularly perturbed problems, *Numer. Math.*, 109 (2008), 167–191.
- [11] H. S. Dollar, N. I. M. Gould, M. Stoll & A. J. Wathen, Preconditioning saddle-point systems with applications in optimization, *SIAM J. Sci. Comput.*, 32 (2010), 249–270.
- [12] I. Duff, MA57 — a code for the solution of sparse symmetric definite and indefinite systems. *ACM Trans. Math. Software*, 30 (2004), 118–154.
- [13] H. C. Elman, D. J. Silvester & A. J. Wathen, Finite elements and fast iterative solvers: with applications in incompressible fluid dynamics. Oxford University Press, New York, 2005.

- [14] S. Franz, R. B. Kellogg & M. Stynes, Galerkin and streamline diffusion finite element methods on a Shishkin mesh for a convection-diffusion problem with corner singularities, *Math. Comp.*, 81 (2012), 661–685.
- [15] S. Franz, T. Linß & H.-G. Roos, Superconvergence analysis of the SDFEM for elliptic problems with characteristic layers, *Appl. Numer. Math.*, 58 (2008), 1818–1829.
- [16] S. Franz & G. Matthies, Local projection stabilisation on S-type meshes for convection-diffusion problems with characteristic layers, *Computing*, 87 (2010), 135–167.
- [17] H. Freudenthal, Simplicialzerlegungen von beschränkter Flachheit. *Annals of Mathematics*, 43 (1942), 580–582.
- [18] S. Ganesan & L. Tobiska, Stabilization by local projection for convection-diffusion and incompressible flow problems, *J. Sci. Comput.*, 43 (2010), 326–342.
- [19] B. García-Archilla, Shishkin mesh simulation: Complementary experiments. (Typescript).
- [20] N. I. M. Gould, J. A. Scott, Jennifer & Y. Hu, A numerical evaluation of sparse direct solvers for the solution of large sparse symmetric linear systems of equations, *ACM Trans. Math. Software*, 33 (2007), 2, Art. 10, 32 pp.
- [21] M. Hagemann & O. Schenk, Weighted matchings for preconditioning symmetric indefinite linear systems, *SIAM J. Sci. Comput.*, 28 (2006), 403–420.
- [22] P. W. Hemker, A singularly perturbed model problem for numerical computation. *J. Comput. Appl. Math.*, 76 (1996), 277–285.
- [23] P. Houston, C. Schwab & E. Süli, Discontinuous hp-finite element methods for advection-diffusion-reaction problems, *SIAM J. Numer. Anal.*, 39 (2002), 2133–2163.
- [24] T. J. R. Hughes, L. P. Franca & G. M. Hulbert, A new finite element formulation for computational fluid dynamics. VIII. The Galerkin/least-squares method for advective-diffusive equations. *Comput. Methods Appl. Mech. Engrg.*, 73 (1989), 173–189.
- [25] V. John, A numerical study of a posteriori error estimators for convection-diffusion equations, *Comput. Methods Appl. Mech. Engrg.*, 190 (2000), 757–781.
- [26] V. John & P. Knobloch, On spurious oscillations at layers diminishing (SOLD) methods for convection-diffusion equations: Part I — A review, *Comput. Methods Appl. Mech. Engrg.*, 196 (2007), 2197–2215.

- [27] V. John, P. Knobloch & S. B. Savescu, A posteriori optimization of parameters in stabilized methods for convection-diffusion problems - Part I, *Comput. Methods Appl. Mech. Engrg.*, 200 (2011), 2916–2929.
- [28] N. Kopteva & E. O’Riordan, Shishkin meshes in the numerical solution of singularly perturbed differential equations, *Int. J. Numer. Anal. Model.*, 7 (2010), 393–415.
- [29] H. W. Kuhn, Some combinatorial lemmas in topology. *IBM J. Res. Develop.*, 45 (1960), 518–524.
- [30] N. Madden & M. Stynes, Linear enhancements of the streamline diffusion method for convection-diffusion problems, *Computers Math. Applic.*, 32 (1996), 29–42.
- [31] J. J. H. Miller, E. O’Riordan & G. I. Shishkin, *Solution of Singularly Perturbed Problems with ε -uniform Numerical Methods - Introduction to the Theory of Linear Problems in One and Two Dimensions*. World Scientific, Singapore, 1996.
- [32] T. Linß, Uniform superconvergence of a Galerkin finite element method on Shishkin-type meshes, *Numer. Methods Partial Differential Equations*, 16 (2000), 426–440.
- [33] T. Linß & M. Stynes, The SDFEM on Shishkin meshes for linear convection-diffusion problems, *Numer. Math.*, 87 (2001), 457–484.
- [34] C. C. Paige & M. S. Saunders, Solution of sparse indefinite systems of linear equations, *SIAM J. Numer. Anal.*, 12 (1975), 617–629.
- [35] G. R. Richter, The discontinuous Galerkin method with diffusion, *Math. Comp.*, 58 (1992), 631–643.
- [36] H.-G. Roos, M. Stynes & L. Tobiska, *Robust Numerical Methods for Singularly Perturbed Differential Equations Convection-Diffusion-Reaction and Flow Problems*, Springer, 2008.
- [37] G. I. Shishkin, *Grid Approximation of Singularly Perturbed Elliptic and Parabolic Equations*. Second doctoral thesis, Keldysh Institute, Moscow, 1990. In Russian.
- [38] M. Stynes, Steady-state convection-diffusion problems, *Acta Numer.*, 14 (2005), 445–508.
- [39] M. Stynes & E. O’Riordan, A uniformly convergent Galerkin method on a Shishkin mesh for a convection-diffusion problem, *J. Math. Anal. Appl.*, 214 (1997), 36–54.
- [40] O. Schenk & K. Gärtner, On fast factorization pivoting methods for symmetric indefinite systems, *Elec. Trans. Numer. Anal.*, 23 (2006), 158–179.

- [41] O. Schenk, A. Wächter & M. Hagemann, Matching-based preprocessing algorithms to the solution of saddle-point problems in large-scale nonconvex interior-point optimization, *Comput. Optim. Appl.*, 36 (2007), 321–341.
- [42] O. Schenk, A. Wächter & M. Weiser, Inertia-revealing preconditioning for large-scale nonconvex constrained optimization, *SIAM J. Sci. Comput.*, 31 (2008/09), 939–960.
- [43] M. Stynes & L. Tobiska, The SDFEM for a convection-diffusion problem with a boundary layer: optimal error analysis and enhancement of accuracy, *SIAM J. Numer. Anal.*, 41 (2003), 1620–1642.
- [44] P. Sun, L. Chen & J. Xu, Numerical studies of adaptive finite element methods for two dimensional convection-dominated problems, *J. Sci. Comput.*, 43 (2010), 24–43.
- [45] M. Tabata, A finite element approximation corresponding to the upwind differencing, *Memoirs Numer. Math.*, 1 (1977), 47–63.
- [46] C. Xenophontos & S. R. Fulton, Uniform approximation of singularly perturbed reaction-diffusion problems by the finite element method on a Shishkin mesh, *Numer. Methods Partial Differential Equations*, 19 (2003), 89–111.
- [47] Zh. Zhang, Finite element superconvergence on Shishkin mesh for 2-d convection-diffusion problems, *Math. Comp.*, 72 (2003), 1147–1177.

Shishkin mesh simulation: Complementary experiments

Bosco García-Archilla²

June 7, 2021

Abstract

We present here some of the experiments that, for the sake of brevity were not included [3]. *The present paper is neither self-contained nor intended to be published in any major journal*, but is intended to be accessible to anyone wishing to learn more on the performance of the SMS method. It should be read as a complement to [3].

1 Numerical experiments

In its present version, this document is not selfcontained, and its contents must be seen as add ons to [3]. Recall that in that paper we are concerned with

$$-\varepsilon \Delta u + b \cdot \nabla u + cu = f, \quad \text{in } \Omega, \quad (1)$$

$$u = g_1, \quad \text{in } \partial\Omega_D, \quad \frac{\partial u}{\partial n} = g_2, \quad \text{in } \partial\Omega_N, \quad (2)$$

where Ω is a bounded domain in \mathbb{R}^d , $d = 1, 2, 3$, its boundary $\partial\Omega$ being the disjoint union of Γ_D and Γ_N , b and c are given functions and $\varepsilon > 0$ is a constant diffusion coefficient.

Example 1 *Simulation of Shishkin grids.* Let us also mention that we rerun the SUPG-based SMS manually tuning the streamline diffusion parameter and found that, in this example, if set 1.5 times larger than the value shown in [3, Fig. 11], the errors improve by a factor of two approximately, resulting in the most efficient method and at least twice as efficient as the SUPG on Shishkin grids

Example 2 *Comparisons on the same grid.* The difference between the SUPG and the SMS methods is even larger when errors are measured in the H^1 norm, which are shown in Fig. 1

Example 3 *Irregular grids on curved domains.*

²Departamento de Matemática Aplicada II, Universidad de Sevilla, Sevilla, Spain. Research supported by Spanish MEC under grant MTM2009-07849 (bosco@esi.us.es)

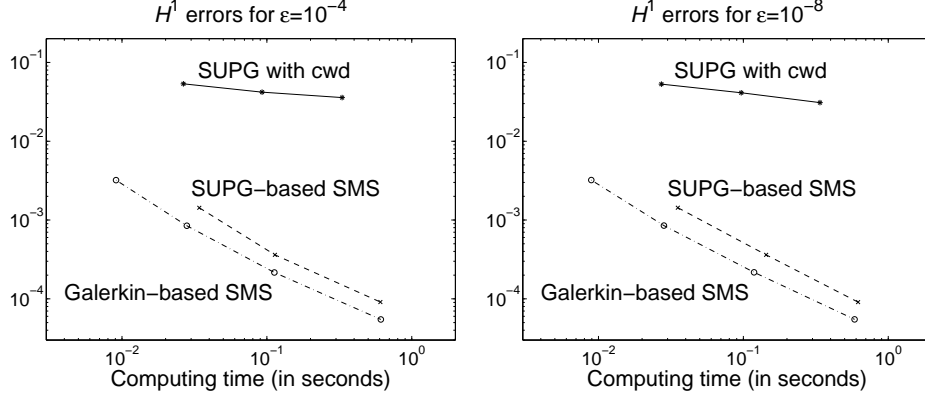


Figure 1: Relative efficiency of SMS and SUPG (with crosswind diffusion) methods in the H^1 norm.

We study the behaviour of SMS methods on irregular grids. For a given positive integer N , we consider grids with $(N+1)^2$ points in $\overline{\Omega}$, where $4N$ of them are randomly distributed on $\partial\Omega$. Let us denote by N_o the number of these on Γ_D^{0+} . Then, in from the remaining $(N-1)^2$ points, N_o of them are displaced by the normal vector from those on Γ_D^{0+} (this is done to create a strip of elements on the outflow boundary) and the rest are generated randomly according to the following two schemes.

Highly irregular grids The points are generated following uniform distribution on the square enclosing Ω , and those enclosed by $\partial\Omega$ and the outflow strip are included in the grid until the desired number $(N-1)^2 - N_o$ of them is reached.

Mildly irregular grids A uniform grid is build first inside Ω and the outflow strip, its diameter h in the x and y direction being the value for which the number of points is the closest to $(N-1)^2 - N_o$. Then each point is displaced randomly on the x and y directions with a uniform distribution on $[-h/3, h/3]$. This is the type of grid used in the experiments in [3].

An example with the two types of grids can be seen in Fig. 4.

For different values of N , we generated 200 random grids of both types, and on each of them we computed the SUPG and SMS approximations and their L^2 error in the convective derivative in $\hat{\Omega}_h$, that is

$$\|b \cdot \nabla w_h - 1\|_{L^2(\hat{\Omega}_h)},$$

for $w_h = u_h$ the SUPG approximation and $w_h = \tilde{u}_h$, the SMS approximation (both Galerkin and SUPG-based). The errors on the 200 grids for $N = 80$ and $\varepsilon = 10^{-8}$ are depicted in Fig. 2. They are marked with a dot, an asterisks

and a cross for the SUPG, Galerkin-based SMS and SUPG-based SMS methods, respectively. The results have been reordered so that those of the SUPG method appear in descending order. As in the results shown in [3], the SMS

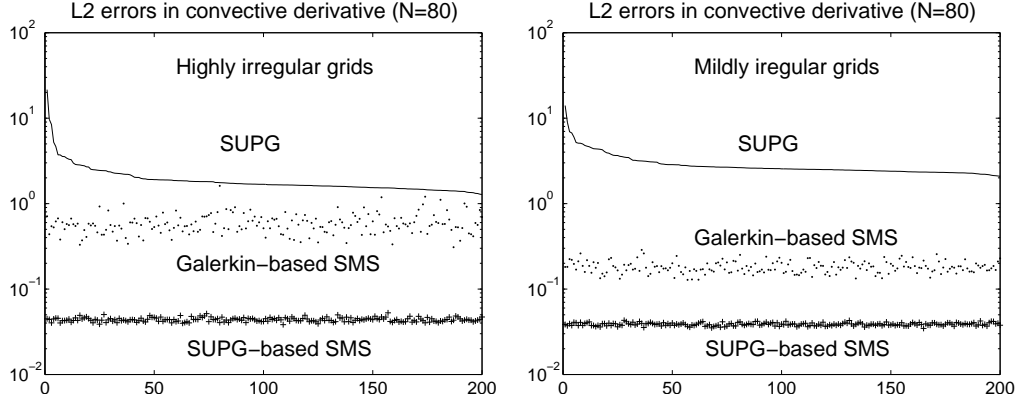


Figure 2: Errors in convective derivative on random grids.

methods clearly improve the error with respect the SUPG method, particularly so in the case of the SUPG-based SMS method. Computing the ratios of the error of the SUPG method and each of the SMS methods and taking the arithmetic mean, the resulting values are for the Galerkin-based and SUPG-based SMS methods, respectively, 5.17 and 65.57 on highly irregular grids, and 16.30 and 75.16 on mildly irregular grids. That is, the SMS methods commit errors that are, on average, between 5 and 75 times smaller than those of the SUPG method.

In Fig. 2 we can also see that while the SUPG and SUPG-based SMS methods are insensitive to the irregularity of the grids, this is not the case of the Galerkin-based SMS method. This is also reflected on Fig. 3, where we show the worst cases of Galerkin-based SMS method on both types of random grids for $N = 40$: whereas in the highly irregular grids the approximation exhibits oscillations, this not so noticeable on the mildly irregular grid (the corresponding grids are shown in Fig. 4). As commented in [3], some results explaining the degradation of performance of the Galerkin method on irregular grids can be found in [1] and [5]. However, we must remark that the approximation on the left plot in Fig. 3 is the worst case out of 200, and that in most of the cases on highly-irregular grids the Galerkin-based SMS method did not present spurious oscillations. Nevertheless, due to the better performance of the Galerkin-based SMS method on mildly-irregular grids, in the rest of the paper, we will only deal with either regular or mildly-irregular grids.

We show the arithmetic mean of the errors committed by the different methods on mildly irregular grids for each value of N in Fig. 5. We also show the

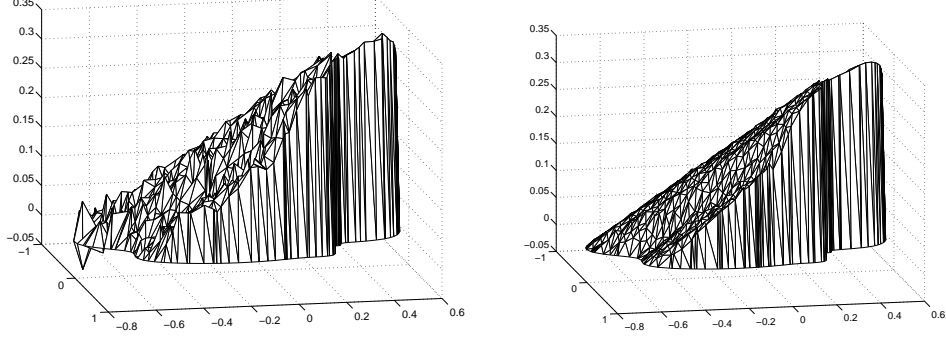


Figure 3: The worst cases of the Galerkin-based SMS method for $N = 40$ on highly irregular and mildly irregular grids (left and right, respectively).

slopes of least-squares fits to the different sets of results. We observe that the errors in the SUPG-based SMS method decay as the meshes become finer (at a rate of $N^{-0.6}$) marginally so in the case of the Galerkin-based SMS method and they grow in the SUPG method. That is, the SUPG method has not reached the convergence regime yet for these meshes in this problem. We can have an idea of why the errors grow by looking at Fig. 6, where we show the SUPG approximation on the grids shown in Fig. 4 (compare with the Galerkin-based SMS in Fig. 3). We notice that large amplitude of the oscillations near the outflow boundary. The large amplitude of the oscillations decreases slower than the grid size, so that the errors in the convective derivative grow.

Example 4 *Parabolic Layers*. Recall that in [3] we solve (1) on $\Omega = (0, 1)^2$, with $\varepsilon = 10^{-8}$, $b = [1, 0]^T$ and f constant equal to 1 with Dirichlet homogeneous boundary conditions. The solution has one exponential layer at $x = 1$ and two parabolic layers along $y = 0$ and $y = 1$.

In [4], a random grid is used and the sets $\Omega_2 = (0, 0.9) \times (0, 0.1]$ and $\Omega_3 = (0, 0.9) \times [0.9, 1]$, and $\Omega_4 = [0.9, 1) \times (0.1, 0.9)$ are considered, and the following quantities computed for numerical approximations w_h :

$$\text{osc}_{\text{para}(2)} := \max \left\{ \max_{(x_s, y_s) \in \Omega_2} -\partial_y w_h(x_s, y_s), \max_{(x_s, y_s) \in \Omega_3} \partial_y w_h(x_s, y_s) \right\}, \quad (3)$$

$$\text{osc}_{\text{exp}} := \max_{(x_s, y_s) \in \Omega_4} \partial_x w_h(x_s, y_s) \quad (4)$$

(x_s, y_s) being the barycenters of the triangles. The optimal values for $\text{osc}_{\text{para}(2)}$ and osc_{exp} are, respectively, 0 and 1, the larger these values are, the stronger are the oscillations in the characteristic and exponential layers, respectively. None of the methods tested in [4] presents a value of $\text{osc}_{\text{para}(2)}$ below 10^{-2} , nor a value of osc_{exp} that is less than 10^{-2} away from the target value 1. We try 200 random irregular grids with 1681 interior grid points (the grid in [4] had

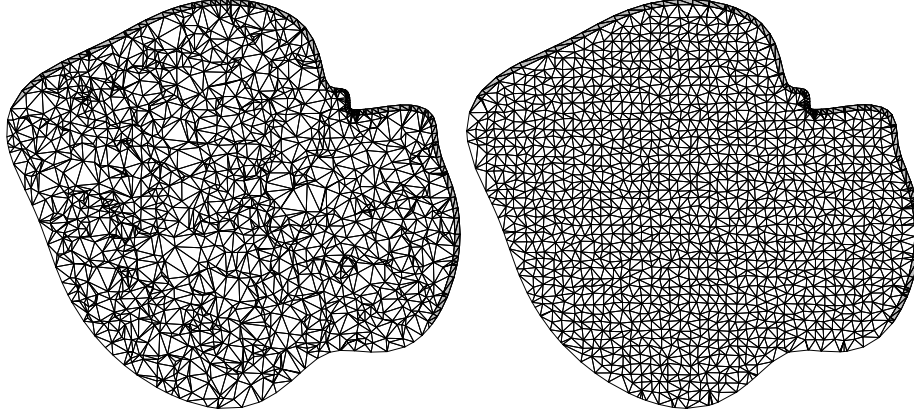


Figure 4: The grids of the plots in Fig. 3. The set Ω_h^+ is shadowed in grey and the points in \mathcal{N}_δ are marked with a dot.

1721), which were created as in Example 3. On these grids, the highest values of $\text{osc}_{\text{para}(2)}$ and $|\text{osc}_{\text{exp}} - 1|$ in the SMS methods were, respectively, 2.9×10^{-13} and 2.8×10^{-13} . Similar striking differences were observed in the rest of the quantities measured in [4] in this example.

Also, with highly irregular grids, as long as they had a strip of elements along Γ_D^{0+} , the results were similar to those of mildly-irregular grids.

Example 5 *Interior layers.* Nothing to be added here at this stage. This example is revisited after Example 6 below.

Example 6 *Hemker problem.* We test the technique to include the layer characteristic in the grid that was proposed in [3, Example 6]. To do this, we change b and the boundary conditions to

$$b = \begin{bmatrix} \cos(\theta) \\ \sin(\theta) \end{bmatrix}, \quad u(x, y) = \begin{cases} 0, & \text{if } x = -3 \text{ or } y = -3, \\ 1, & \text{if } x^2 + y^2 = 1, \\ \varepsilon \nabla u \cdot n = 0, & \text{elsewhere} \end{cases} \quad (5)$$

for $\theta \in (0, \pi/4]$. (The boundary conditions are changed so that the inflow boundary Γ^- is part of the Dirichlet boundary Γ_D). The idea is to try different combinations of characteristic layers and grid alignments. In the following computations, the enlarged grids and the corresponding sets Ω_h^+ can be as irregular as those depicted in Fig. 7. To prevent elements with one side parallel to b being downwind of Ω_h^+ (see [3, Section 3.2.2] for the possible adverse effects of this) when $\theta = \pi/4$ we red-refined all triangles in Ω_h^+ along the interior layers. Otherwise, no extra provisions were taken in the computations that follow, except removing isolated components in $\hat{\Omega}_h$ (when present) as explained in [3, Section 3.2.2].

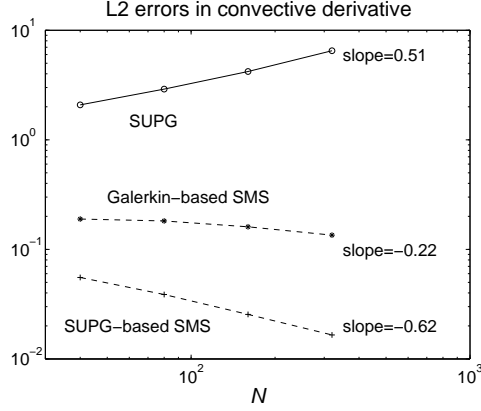


Figure 5: Arithmetic means of the errors on mildly irregular grids.

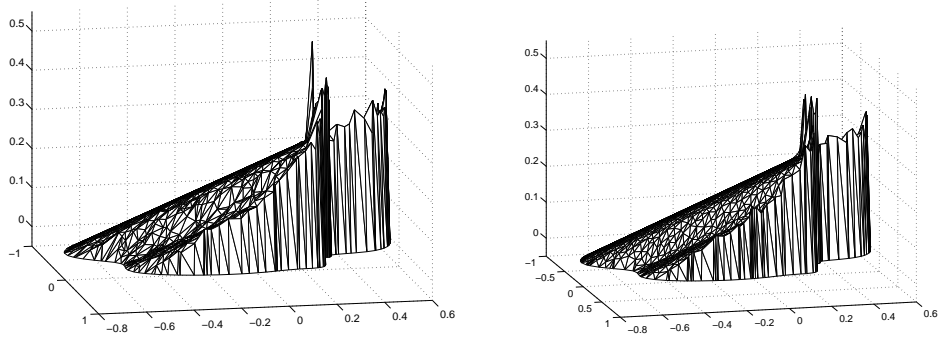


Figure 6: The SUPG approximation on the grids shown in Fig. 4.

We considered 100 equidistant values of θ in $(0, \pi/4]$. For each of them we computed the overshoots and undershoots of the SUPG and SMS approximations on the grid depicted in [3, Fig. 20]. For the SUPG and the Galerkin-based SMS approximations, Fig. 8 shows the difference between the overshoots and undershoots, as a measure of the oscillations in each method (the results of the SUPG-based SMS method were similar to those of the Galerkin-based method and are not shown). We see that out of the 100 values of θ tried, only in four of them are the oscillation on the SMS method larger than 10^{-12} , the arithmetic mean of these four values being 0.013, yet well below the average value in the SUPG method, 0.65.

We investigate the reason of those four cases presenting values of over and undershoots so different to the rest of the cases. The reason is that some mesh points of the enlarged grid are too close to the interior layer, and this results

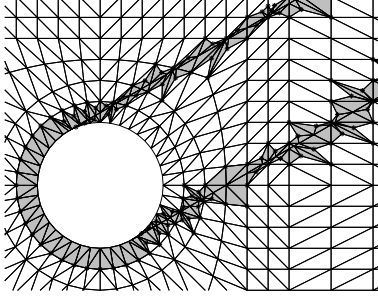


Figure 7: Detail of the enlarged grid, the set Ω_h^+ (shadowed in grey) and the points in \mathcal{N}_δ (marked with asterisks) in Example 6 for $\theta = \pi/6$ in (5).

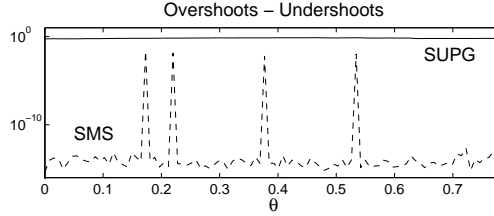


Figure 8: Difference between the over and undershoots for the approximations on the grid depicted in [3, Fig. 20] in Example 6, with b and boundary conditions as specified in (5).

in the set Ω_h^+ being too thin in the neighbourhood of those points. This can be seen in Fig. 9, where on the left plot we show a detail of the enlarged grid (with Ω_h^+ shadowed in grey) for $\theta = 23\pi/400$, which is the first value in Fig. 8 where the overshoots or undershoots are above 10^{-12} in the SMS method. The center plot is a magnification of the left one around the point too close to the layer characteristic, where we can see that very stretched triangles have been created on the enlarged grid. If we move the point to the layer characteristic, the resulting set Ω_h^+ is shown in the right plot of Fig. 9, and we can see it is much wider than that in the left plot.

We repeated the four cases in the SMS method where oscillations were much larger than the rest of the cases, but this time allowing a vertex v of a triangle τ to move to the layer characteristic if its distance to it was less than $(h_{\min}(\tau))^2/10$, where $h_{\min}(\tau)$ is the minimum distance between the vertices of τ . Once the SMS approximations were computed on the moved grids, values on the unmoved grid were computed by interpolation and over and undershoots were again computed. The overshoots in all cases turned out to be below 10^{-14} , and the undershoots were zero in all cases. Notice that when not altering the grid (not even by less than $h_{\min}^2/10$) is an important issue, then, another option to avoid mesh points

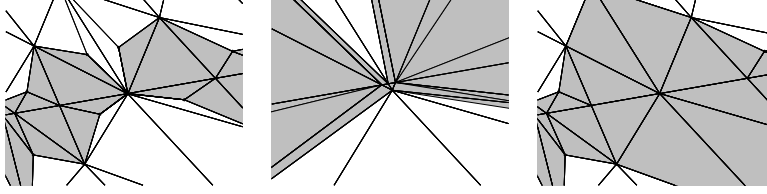


Figure 9: Left: detail of the enlarged grid and Ω_h^+ for $\theta = 23\pi/400$ in Example 6 with (5). Center: magnification of the left plot around a point too close to the characteristic layer. Right: the set Ω_h after moving that point to the layer characteristic.

too close to the layer characteristic is to slightly perturb the wind velocity b in the neighbourhood of those points so that the layer characteristic passes through them.

Example 5 (revisited). As in example 4, we compute with our method some of the quantities used in [4] to measure the quality of the approximations. For an approximation $w_h \in V_h$, these are

$$\text{osc}_{\text{int}} := \left(\sum_{(x,y) \in \Omega_1} (\min\{0, w_h(x,y)\})^2 + (\max\{0, w_h(x,y) - 1\})^2 \right)^{1/2}, \quad (6)$$

$$\text{smear}_{\text{int}} := x_2 - x_1, \quad (7)$$

where $\Omega_1 = \{(x,y) \in \Omega \mid x \leq 0.5, y \geq 0.1\}$, and x_1 and x_2 are the first points on the line $y = 0.25$ satisfying, respectively, $w_h(x_1, 0.25) \geq 0.1$ and $w_h(x_2, 0.25) \geq 0.9$. It is argued in [4] that (7) is a measure of the thickness of the interior layer. Observe also that the target value for osc_{int} is 0.

We computed the value of these quantities in the case of the SMS approximations on a regular 64×64 grid with Southwest-Northeast diagonals, using the technique of the previous example to include the layer characteristic in the grid. On a similar mesh, out of 18 methods tested in [4] the value of osc_{int} was larger than 0.1 in 14 of them, and larger than 0.001 in three more of them. In contrast, the value of osc_{int} in the SMS methods was 1.8×10^{-14} (Galerkin-based) and 2.2×10^{-13} (SUPG-based). Also, the value of $\text{smear}_{\text{int}}$ was larger than 6.2×10^{-2} in all the methods tested in [4], whereas for both SMS methods was 1.3×10^{-2} . For the SUPG method, the values of osc_{int} and $\text{smear}_{\text{int}}$ were, respectively, 0.59 and 0.062, the same values as in [4].

On the irregular grid in [4], they obtain results were very similar to those of the regular grid. We, on our part, tried the 200 random grids of Example 4 in the present one. The mean value $\text{smear}_{\text{int}}$ in the SMS methods was 2.7×10^{-2} . With respect the value of osc_{int} in the SMS methods, out of the 200 runs, in only 20 of them was this value larger than 10^{-8} , being the mean value in these 20 cases of 0.1822, which still compares very favourable with most of the methods tested in [4]. We rerun these 20 cases allowing a grid points to move to the layer

characteristic if the distance to it was less $2h_{\min}^2$, and in 19 of them the value of osc_{int} move to under 10^{-10} . In the remaining case this was also achieve if we red-refining the triangles in Ω_h^+ next to the inner layer characteristic.

Example 7 *Double-glazing test problem* [2]. Whatever we may have to add in this case will be reported elsewhere.

References

- [1] L. Chen & J. Xu, Stability and accuracy of adapted finite element methods for singularly perturbed problems, *Numer. Math.*, 109 (2008), 167–191.
- [2] H. C. Elman, D. J. Silvester A. J. Wathen, *Finite elements and fast iterative solvers: with applications in incompressible fluid dynamics*. Oxford University Press, New York, 2005.
- [3] B. García-Archilla, Shiskin mesh simulation: A new stabilization technique for convection-diffusion problems, *Comput. Methods Appl. Mech. Engrg.*, 256 (2013), 1–16.
- [4] V. John & P. Knobloch, On spurious oscillations at layers diminishing (SOLD) methods for convection-diffusion equations: Part I — A review, *Comput. Methods Appl. Mech. Engrg.*, 196 (2007), 2197–2215.
- [5] P. Sun, L. Chen & J. Xu, Numerical studies of adaptive finite element methods for two dimensional convection-dominated problems, *J. Sci. Comput.*, 43 (2010), 24–43.